

1 Dear Prof. Carslaw,
2
3 On behalf of all authors I would like to thank you again for taking the time to
4 edit our manuscript.
5
6 As requested a native English speaker looked over the manuscript.
7 The following major changes have been made (marked in red in the
8 manuscript below):
9 The sentence starting on p.6, line 15 has been rephrased.
10 The sentence starting on p.12, line 24 has been rephrased.
11 The sentence starting on p.13, line 13 has been rephrased.
12 The sentences starting on p.17, line 30 to p.18, line 2 have been rephrased.
13 The figure captures have been revised.
14 The paragraph starting on p.16, line 17 has been rewritten in order to clarify
15 that the fragmentation mechanisms in the atmosphere are not well
16 established. Part of the final sentence of this paragraph has been moved to
17 the footnote on p.5.
18
19 We hope that the quality of writing in the manuscript has improved and is
20 sufficient for publication in ACP now.
21
22 Yours sincerely,
23 Evelyne Hamacher-Barth
24 |

1 **Size resolved morphological properties of the high**
2 **Arctic summer aerosol during ASCOS-2008**

3

4 **E. Hamacher-Barth¹, C. Leck¹ and K. Jansson²**

5 [1] {Department of Meteorology, Stockholm University, Stockholm, Sweden}

6 [2] {Department of Materials and Environmental Chemistry, Stockholm
7 University, Stockholm, Sweden}

8 Correspondence to: E. Hamacher-Barth (evelyne@misu.su.se)

9

10 **Abstract**

11 The representation of aerosol properties and processes in climate models is fraught
12 with large uncertainties. Especially at high northern latitudes a strong under-
13 prediction of aerosol concentrations and nucleation events is observed and can only be
14 constrained by in situ observations based on the analysis of individual aerosol
15 particles. To further reduce the uncertainties surrounding aerosol properties and their
16 potential role as cloud condensation nuclei this study provides observational data
17 resolved over size on morphological and chemical properties of aerosol particles
18 collected in the summer high Arctic, north of 80° N.

19 Aerosol particles were imaged with scanning and transmission electron microscopy
20 and further evaluated with digital image analysis. In total, 3909 aerosol particles were
21 imaged and categorized according to morphological similarities into three gross
22 morphological groups: single particles, gel particles and halo particles. Single
23 particles were observed between 15 and 800 nm in diameter and represent the
24 dominating type of particles (82%). The majority of particles appeared to be marine
25 gels with a broad Aitken mode peaking at 70 nm and accompanied by a minor
26 fraction of ammonium (bi)sulfate with a maximum at 170 nm in number
27 concentration. Gel particles (11% of all particles) were observed between 45 and 800
28 nm with a maximum at 154 nm in number concentration. Imaging with transmission
29 electron microscopy allowed further morphological discrimination of gel particles in
30 “aggregate” particles, “aggregate with film” particles and “mucus-like” particles.

1 Halo particles were observed above 75 nm and appeared to be ammonium (bi)sulfate
2 (59% of halo particles), gel matter (19%) or decomposed gel matter (22%), which
3 were internally mixed with sulfuric acid, methane sulfonic acid or ammonium
4 (bi)sulfate with a maximum at 161 nm in diameter.

5 Elemental dispersive X-ray spectroscopy analysis of individual particles revealed
6 prevalence of the monovalent ions Na^+/K^+ for single particles and “aggregate”
7 particles and of the divalent ions $\text{Ca}^{2+}/\text{Mg}^{2+}$ for “aggregate with film” particles and
8 “mucus-like” particles. According to these results and other model studies, we
9 propose a relationship between the availability of Na^+/K^+ and $\text{Ca}^{2+}/\text{Mg}^{2+}$ and the
10 length of the biopolymer molecules participating in the formation of the 3D gel
11 networks.

12 1 Introduction

13 Aerosol particles have major impacts on the climate of our planet. They alter the
14 planetary albedo both directly by absorbing and scattering sunlight and indirectly by
15 modifying the reflectivity, life-time and extent of clouds (Twomey, 1977; Albrecht,
16 1989; Solomon et al., 2007). Despite the known importance of the effects of aerosol
17 particles on clouds, they still give rise to large uncertainties in climate models
18 (Schimel et al., 1996; Penner et al., 2001; Forster et al., 2007). Detailed model
19 analyses have contributed to an enhanced understanding of the parametric
20 uncertainties in global aerosol models and point towards significant uncertainties
21 arising from an incomplete representation of aerosol processes and emissions in the
22 models (e.g., Lee et al., 2013; Carslaw et al., 2013; Mann et al., 2014). Especially for
23 high northern latitudes, a strong under-prediction of aerosol particle concentrations
24 and nucleation events in summer compared to measurements is recognized (Mann et
25 al., 2014). This can lead to an insufficient representation of cloud condensation nuclei
26 (CCN), which can activate and form cloud droplets, in models. Moreover, the
27 microphysical properties of the cloud droplets are strongly related to the size,
28 chemical composition, morphology and state of mixture of the activated CCN. Size
29 resolved data based on the analysis of individual particles are therefore indispensable
30 for an appropriate parameterization of aerosol particles within aerosol models.

31 The sources of aerosol particles in the Arctic are subjected to large regional and
32 seasonal differences. In late winter/spring, a pronounced anthropogenic influence on
33 the Arctic is observed, that is a phenomenon known as Arctic haze (Shaw, 1995).

1 During that time the Arctic air mass expands southwards towards Eurasia and North
2 America and anthropogenic emissions are transported into the Arctic where they
3 remain for prolonged times (Shaw, 1995; Douglas and Sturm, 2003). The aerosol
4 during periods of Arctic haze is characterised by relatively high concentrations of
5 aged aerosol predominantly in the accumulation mode (Shaw, 1984; Heintzenberg
6 and Leck, 1994; Ström et al., 2003; Engvall et al., 2008; Korhonen et al., 2008). The
7 air masses arriving in summer, however, originate from sectors over the oceans with
8 limited man-made activities and the transport into the Arctic is slower compared to
9 winter conditions (Stohl, 2006). The summer conditions are thus much more pristine
10 and the aerosol shifts from a dominance of the accumulation mode to the Aitken mode
11 (Heintzenberg et al., 2006; 2015; Engvall et al., 2008).

12 Over the high Arctic pack ice north of 80° number concentrations of CCN show a
13 large temporal variability, ranging over 2 to 3 orders of magnitude but usually are
14 below 100 cm⁻³ and occasionally less than 1 cm⁻³ (Lannefors et al., 1983; Bigg et al.,
15 Bigg and Leck, 2001a; Mauritzen et al., 2011; Leck and Svensson, 2015). These
16 relatively low CCN concentrations have a significant impact on the formation of low-
17 level (stratiform) clouds prevalent in the high Arctic summer. Mauritzen et al. (2011)
18 identified a regime with very low CCN concentrations (< 10 cm⁻³) where cloud
19 formation is limited mainly by the availability of CCN. Such low CCN concentrations
20 occur as a result of weak local aerosol sources and effective wet deposition (Nilsson
21 and Leck, 2002; Held et al., 2011a,b; Heintzenberg et al., 2006; Leck and Svensson,
22 2015) at the marginal ice zone and over the pack ice.

23 The physical and chemical properties which determine the ability of the summer high
24 Arctic aerosol particles to act as CCN are still not very well understood. Attempts to
25 theoretically predict concentrations of CCN in closure studies resulted in over- and
26 under-predictions of the observed CCN concentrations (Zhou et al., 2001; Bigg and
27 Leck, 2001a; Lohman and Leck, 2005; Martin et al., 2011; Leck and Svensson, 2015).
28 The most recent closure study by Leck and Svensson (2015) simulated the cloud
29 nucleation process by assuming Köhler theory together with a Lagrangian adiabatic
30 air parcel model that solves the kinetic formulation for condensation of water on size-
31 resolved aerosol particles. The authors suggested a larger fraction of the
32 internally/externally mixed water-insoluble particles in the smaller aerosol size ranges
33 as well as and kinetically restricted growth of the activated particles. The non-water
34 soluble particle fraction was suggested to physically and chemically behave as

1 polymer gels¹ with a dichotomous behavior (low hygroscopic growth factor but a high
2 CCN activation efficiency) in cloud droplet activation as a result of the interaction of
3 the hydrophilic and hydrophobic entities on the structures of the high Arctic polymer
4 gels (Orellana et al., 2011). On average 32% of the Arctic surface ocean DOM
5 assembled as microgels (Orellana et al., 2011), a significantly higher percentage than
6 reported for other ocean regions (10%; Chin et al., 1998; Verdugo et al., 2004). All
7 together these findings strongly supported the previously unverified hypothesis of a
8 link between cloud formation and polymer gels in the surface microlayer (SML, <
9 1000 μm thick at the air-sea interface) of the high Arctic open leads (Bigg et al., 2004;
10 Leck and Bigg, 1999; Leck et al., 2002; Leck and Bigg, 2005b; Bigg and Leck, 2008;
11 Leck and Bigg, 2010).

12 The transport of marine gels into the atmosphere is thought to happen via the burst of
13 air bubbles at the air-sea interface. Air bubbles rising within the water column
14 | scavenge surface-active organic matter, especially from the surface microlayer to their
15 outer walls (Wotton and Preston, 2005). Bursting of the bubbles at the water surface
16 produces small jet and film drops containing organic surface-active compounds,
17 debris of phytoplankton, bacteria, viruses and sea salt (Blanchard and Woodcock,
18 1957; Blanchard, 1971, Blanchard and Syzdek, 1988; Gershey, 1983; O'Dowd et al.,
19 | 1999), that are transported further up into the atmosphere through turbulent mixing
20 processes. However, studies of individual particles by Bigg and Leck (2001; 2008);
21 Leck et al., (2002); Leck and Bigg (2005a; 2005b) over the perennial ice have failed
22 to find evidence of sea salt particles of less than 200 nm in diameter. In the Arctic
23 breaking waves as a source of bubbles are rare due to low wind speeds and short
24 fetches between the ice floes (Tjernström et al., 2012). Even in the absence of wind-
25 driven breaking waves a recent study has now confirmed both the presence and
26 temporal variability of a population of bubbles within the open leads (Norris et al.,
27 2011). The considered mechanisms for bubble formation and mixing were induced by
28 changes in gas saturation. Other possible bubble formation mechanisms are
29 respiration from algae and phytoplankton (Medwin, 1970; Johnson and Wangersky,
30 1987) and the release of trapped air from melting ice (Wettlaufer, 1998).

¹ Phytoplankton and bacteria in surface seawater produce varying amounts of mucus- or gel-like matter comprised of biopolymers like proteins, polysaccharides or lipids that form 3-dimensional networks inter-bridged with divalent ions, preferably Ca^{2+} and Mg^{2+} . [Embedded in the polymer network is a high content of water \(99%\) that prevents the network from collapsing \(Chin et al., 1998\)](#). This type of supramolecular organisation is referred to as marine gels. (Verdugo, 2012 gives a review).

1 Due to the remoteness and the harsh conditions in the high Arctic, the number of
2 aerosol studies from this region is limited with data available only from four
3 expeditions onboard the Swedish icebreaker *Oden* during the summers of 1991, 1996,
4 2001 and 2008 (Leck et al., 1996; 2001, 2004; Tjernström et al., 2014). These
5 expeditions took advantage of the pristine conditions during the Arctic summer when
6 the Arctic is greatly separated from polluted mid-latitudinal sources, which provided a
7 unique opportunity to study aerosol particles from predominantly natural sources. All
8 other Arctic studies on aerosol chemical composition, morphology and state of
9 mixture were either performed during winter/spring when the transport of polluted
10 aerosol from lower latitudes into the high Arctic was strong (e.g. Hara et al., 2003;
11 Xie et al., 2007; Winiger et al., 2015) and/or they were located further south and
12 outside of the pack ice area. The latter event would allow missing potential aerosol
13 sources from the pack-ice area and at the same time include anthropogenic pollutions
14 (e.g. Geng et al., 2010; Chi et al., 2015).

15 An investigation of size, chemical composition, morphology and state of mixture on
16 the level of individual aerosol particles is required to further reduce the uncertainties
17 surrounding the CCN properties that promote or suppress cloud droplet formation
18 over the pack ice area. The present study will make use of aerosol particles collected
19 during the most recent icebreaker expedition under the name ASCOS (Arctic Summer
20 Cloud and Ocean Study) 2008. The Swedish icebreaker *Oden* departed from
21 Longyearbyen on Svalbard on 2 August and returned on 9 September 2008. After
22 traversing the pack-ice northward, the icebreaker was moored to an ice floe and
23 drifted passively with it around 87° N between 12 August and 1 September
24 (Tjernström et al., 2014). We used electron microscopy (scanning electron
25 microscopy (SEM) and transmission electron microscopy (TEM)) to image aerosol
26 particles at high resolution, and subsequent digital image analysis to objectively
27 assess size and morphology of the particles on an individual basis. Earlier studies
28 north of 80° focused on a qualitative description of the aerosol in the high Arctic
29 (Leck and Bigg, 2005, 2008, 2010; Bigg and Leck, 2001b, 2008) complemented with
30 bulk chemical analyses (Leck et al., 2002; 2013; Leck and Svensson, 2015; Lohman
31 and Leck, 2005).

32 Firstly, by individually screening close to 4000 aerosol particles collected during the
33 ice-drift with SEM and subsequent digital mapping, we gained size resolved
34 information on the aerosol population as a whole. The obtained number size

1 distribution was compared with measurements from an independent method (Tandem
2 Differential Mobility Particle Sizer, TDMPS) to verify that a representative fraction of
3 the aerosol population was captured with SEM. Secondly, we sorted all mapped
4 particles according to morphological differences and a separate number size
5 distribution for each of the morphological types was obtained. Thirdly, to obtain
6 deeper insights into the morphological features of the collected particles and to
7 simultaneously assess their elemental composition with EDX spectroscopy
8 investigated a subpopulation of aerosol particles in TEM at very high resolution.

9

10

1 **2 Methods for sampling of airborne aerosol particles during ASCOS**

2 **2.1 Collection of airborne particles**

3 **2.1.1 The sampling inlet**

4 A PM₁₀-inlet (9 cm inner diameter) was deployed at ambient conditions (85–100 %
5 relative humidity (RH) and temperatures around 0 °C) to eliminate particles with
6 diameters > 10 micrometer in equivalent aerosol dynamic diameter (EAD) from the
7 sampled air. To optimise the distance from the sea-surface and the ship's
8 superstructure, the inlet was located forward 25 m above the sea-surface and 3 m
9 above the roof of the laboratory container on the 4th deck of the icebreaker. Direct
10 contamination from the ship was excluded by using a pollution controller, located
11 directly after the inlet pipe that passed through the roof of the container. Provided that
12 the wind was within ± 70° of the direction of the bow and stronger than 2 ms⁻¹, no
13 pollution reached the sample inlets (Leck et al., 1996). Directly downstream from the
14 pollution sensor the electrostatic precipitator and the TDMPS were connected to the
15 inlet with short stainless steel tubes (length ca. 1 m). To ensure that the sampling
16 conditions and losses were the same for both instruments, the inlet take-offs for the
17 two instruments were placed closely together. The temperature in the container was
18 kept at 20 °C which resulted in an RH of 20% in the secondary lines during sampling.
19 See Leck et al. (2001) for more details of the set-up for the sampling of aerosol
20 particles.

21 Volatile compounds on particle surfaces and weakly bound water molecules were
22 probably lost during the sampling procedure. In the Arctic, the concentration of
23 volatile compounds is generally lower than at lower latitudes (Bates et al., 1987), and
24 losses due to evaporation can be considered very small.

25 **2.1.2 The electrostatic precipitator**

26 Using the electrostatic precipitator the aerosol particles were collected directly onto 3
27 mm copper 300 mesh Formvar-coated TEM grids (TED PELLA Inc.; Dixkens and
28 Fissan, 1999; Leck and Bigg, 2008). Formvar-coated grids were chosen because of
29 the hydrophilic and thus polar nature of the Formvar film (Rocha et al., 2005). The
30 aerosol particles were charged at the inlet of the precipitator by a ⁶³Ni beta-emitting
31 radioactive source and precipitated by a 12 kV cm⁻¹ electric field between the inlet
32 and the collecting grid surface. The flow rate was kept very low (0.17 mL s⁻¹) in order

1 to collect particles up to $\sim 1 \mu\text{m}$ in diameter. The collection efficiency of the
2 electrostatic precipitator was intercompared with a TSI 1236 Nanometer Aerosol
3 Sampler (^{63}Ni beta-emitting radioactive source and sample flow of 1 L m^{-1}) mounted
4 side-by-side with the electrostatic precipitator. Both collected a small but statistically
5 significant number of particles $< 25 \text{ nm}$ in diameter. The precipitator took samples for
6 6 to 12 hrs. Before and after sampling the grids were placed within a grid holder box
7 in a sealed plastic bag and stored in a desiccator at a constant temperature of 20°C .

8 2.1.3 The TDMPS-sampling system

9 The TDMPS-sampling system to measure the number size distributions of dry (20%
10 RH) sub-micrometer particles used pairs of differential mobility analyzers (DMAs).
11 The TSI 3010 counters in the DMAs were size and concentration calibrated against an
12 electrometer and the TSI 3025 counters for particle sizes below 20 nm in diameter
13 according to Stolzenburg (1988). This set up yielded a complete number size
14 distribution from 3 nm to 800 nm diameter scanned over 45 size channels every 10 -
15 20 min. Further details of the TDMPS system can be found in Heintzenberg and Leck
16 (2012). NIST (National Institute of Standards Technology) traceable calibration
17 standards of polystyrene latex spherical particles were used to determine error in
18 determination of the mobility diameter to $\pm 5\%$ (Wiedensohler et al., 2012).

19 In order to compare the number size distribution obtained from the precipitator
20 samples (section 2.1.2) with those simultaneously recorded by the TDMPS we
21 assumed median particle number diameters for each of the 45 TDMPS size channels.
22 The particle diameters were then merged to form a complete set of diameters across
23 the TDMPS measuring interval.

24 2.2 Image recording and elemental analysis

25 2.2.1 Imaging with scanning electron microscopy (SEM)

26 The samples were investigated with a high-resolution SEM (JEOL JSM-7401) under
27 high vacuum conditions, at less than $9.63 \times 10^{-5} \text{ Pa}$ (Stevens et al., 2009). A detailed
28 description of the setup of the scanning electron microscope can be found in
29 Hamacher-Barth et al. (2013). The Gentle Beam mode of the microscope was used to
30 minimize radiation damage of the aerosol particles, avoid surface charge-up and to
31 demagnify the electron beam diameter (Michael et al., 2010). Correction for
32 stigmatism and focusing of the electron beam was done every time before imaging an

1 aerosol particle. The grey scale (contrast and brightness) was adjusted automatically
2 before recording an image.

3 The imaging of the aerosol particles aimed to account for an uneven distribution of
4 the particles on the TEM grid and to capture a representative fraction of the aerosol
5 particles. In brief, particles were imaged at a magnification of 40.000 on the TEM
6 grid squares along a diagonal from the center of the grid to the edge on 6 to 8 squares
7 of the TEM grid. Each square was screened systematically to capture a representative
8 fraction of the aerosol population. For a detailed description of the screening
9 procedure see Hamacher-Barth et al. (2013).

10 **2.2.2 Imaging with transmission electron microscopy (TEM)**

11 To image the samples with TEM they have to be coated by a thin metal layer.
12 Evaporation of a heavy metal thin coating at an oblique angle onto the sample
13 increases the mass contrast and accentuates the topography of the aerosol particle by
14 | producing a shadow (William and Carter, 2006). Furthermore, shading has the
15 advantage that the metal cover protects the aerosol particles against heating by the
16 electron beam during examination, especially at high magnifications. It is also
17 advantageous that in case of any evaporation from the aerosol particle the metal
18 replica of the aerosol particle is still visible.

19 The aerosol particles were shaded with platinum (Pt) at an angle of $\arctan(0.5) = 26^\circ$
20 (Okada, 1983) in a vacuum chamber at 10^{-6} mbar. Pt was evaporated from a Pt wire
21 (\varnothing 0.2 mm, 20 mm length). The Pt wire was drawn around a tungsten (W) wire and
22 evaporated clusters of Pt atoms when the W wire was heated up electrically by a
23 85 mA current for 30 sec. The shading procedure produces a layer of Pt particles of 1-
24 2 nm in diameter on the TEM grid.

25 After shadowing the TEM grids were examined in TEM using a JEOL JEM-2100
26 high-resolution instrument, equipped with a LaB_6 filament and a Si/Li detector crystal.
27 The TEM grid containing the aerosol particles was mounted on a sample holder made
28 of Beryllium to avoid background signals from the sample holder material in the EDX
29 measurements (see chapter 2.2.3). A CCD camera (Gatan SC1000 Orius, 11
30 Megapixel) in bottom mount position was used to image the aerosol particles. Images
31 were taken at high vacuum less than 35×10^{-5} Pa and at an accelerating voltage of
32 100 kV.

1 Particles were imaged on TEM grid squares along a diagonal from the center of the
2 grid to the edge on 6 to 8 squares. To avoid imaging of particles that were damaged
3 by prior imaging with SEM, an area of the grid was chosen, which was not exposed to
4 any electron beam at high magnifications before. Screening each square for individual
5 particles was done at a magnification of 30.000, and images were taken at
6 magnifications between 25.000 and 80.000.

7 **2.2.3 Elemental X-ray spectroscopy**

8 The elemental analyses were performed using an energy dispersive X-ray detector
9 JED-2300 attached to the JEM-2100 TEM. In order to avoid time consuming
10 realignment of the electron beam and focusing procedures, the EDX-analyses were
11 also performed at an accelerating voltage of 100 kV. The energy range measured was
12 0-20 keV, the counting rate was typically 1053 counts/sec⁻¹, the life time was 30 sec,
13 the real time was 33.00 sec and the dead time was 10 %. Generally EDX spectroscopy
14 allows the detection of elements \geq Be as their photon energies are above 100 eV and
15 thus lie within the X-ray region of the electromagnetic spectrum (Egerton, 2008).
16 Nevertheless, the detection of light elements like C, N, and O that are typical for
17 organic compounds can be difficult on a Formvar-coated copper grid since the signal
18 intensity can be biased by attenuation of the X-ray signal through absorption by the
19 adjacent copper grid. For this reason these elements were not reliably detectable and
20 are not part of this study.

21 Blank grids shadowed with platinum were used to identify the background noise and
22 signals from the TEM grid including copper from the grid and the Formvar film and
23 the Pt shadowing. The EDX spectra of blank grids showed only signals from Pt, the
24 supporting copper TEM grid and carbon and oxygen signals from the Formvar
25 substrate-film.

26

27 **2.2.4 Digital image analysis**

28 Images taken with SEM at a magnification of 40.000 were evaluated using an
29 optimized commercial image processing software (AphelionTM Dev 4.10). In brief,
30 the maximal intensity of the neighboring background of each aerosol particle was
31 determined. Using exactly the same image but including the aerosol particle allowed

1 the separation of the particle and measurement of the particle area in pixels
2 (Hamacher-Barth et al., 2013).

3 The particle size was calculated according to Eq. (1)

4
$$D_{pa} = 2 \sqrt{Area/\pi} \quad (1)$$

5 with D_{pa} as the particle equivalent diameter, which is the diameter of a circle that
6 comprises the same area as the aerosol particle projected onto a two-dimensional
7 surface (Allen, 1997; Hinds, 1999). The value for the area is calculated from the
8 number of pixels counted for each particle. A number size distribution of the aerosol
9 sample was obtained using MATLAB 2011a and the freely available software
10 package EasyFit.

11

12 **3 Results and discussion**

13 Firstly, to verify that a representative fraction of the aerosol population has been
14 captured with SEM, we calculated a number size distribution of all aerosol particles
15 and compare it with measurements from TDMPS. Secondly, we sorted all particles
16 imaged according to morphological similarities into three gross groups, named: single
17 particles (SP), gel-like particles (GP) and halo particles (HP), shown in Fig. 2. Thirdly,
18 to obtain more subtle insights into the morphological features of the collected aerosol
19 particles and simultaneously assess their elemental composition we investigated a
20 subpopulation of the aerosol particles with TEM and EDX spectroscopy at very high
21 resolution.

22 **3.1 Total number size distributions**

23 In order to derive an overall number size distribution we imaged in total 3909 aerosol
24 particles at a magnification of 40,000 with SEM. The number size distribution of all
imaged aerosol particles exhibited an Aitken mode at 32 nm in diameter. In the
accumulation mode region maxima are observed at 89 nm and 147 nm with a shoulder
at 335 nm (see Fig. 3, red line). Hamacher-Barth et al. (2013) used the same image
25 mapping method as in this study and determined the error of sizing for polystyrene
26 latex spheres of several diameter sizes between 20 and 900 nm. The error values are
27 displayed in Fig. 3 as red arrows. For the TDMPS number size distribution we
28 assumed an error in determining the mobility diameter of 5% across the whole
29
30
31

1 measuring interval (Wiedensohler et al., 2012). The two approaches show an overall
2 good agreement between their number size distributions with a similar modal
3 structure, an Aitken mode below 80 nm and an accumulation mode at higher
4 diameters. The reduced particle number concentration in the Aitken mode seen by
5 SEM was probably caused by their partly weak contrast to the Formvar film, which
6 either resulted in an underestimation of the size or that the particles remained
7 undetected. The accumulation mode was separated into a double peak with particle
8 number maxima at 89 nm and 147 nm in SEM and 106 nm and 158 nm in diameter in
9 TDMPS. The aerosol particles at diameters > 100 nm often showed a patchy and
10 inhomogeneous appearance, that might have lead to an underestimation of their size
11 and the observed shift to smaller diameters in SEM with that of 147 nm compared to
12 173 nm in TDMPS and broadening of the maximum at 335 nm.

13 In general, the number size distributions determined for particles larger than 20 nm in
14 diameter showed modal features typical for aerosol particles collected in the high
15 Arctic summer boundary layer: an Aitken mode between 26 and 80 nm and a
16 multimodal accumulation mode between 80 and 1000 nm (Covert et al., 1996;
17 Heintzenberg et al., 2006; Heintzenberg and Leck, 2012) with the so called
18 Hoppelminimum around 80 nm in between (Hoppel, 1986).

19 **3.2 Single particles**

20 Single particles (SP) seen by SEM appeared as single entities that mostly contrasted
21 sharply and thus could be easily separated from their Formvar background for
22 diameters > 40 nm. At smaller diameters, however, the contrast to the background was
23 often weak and probably resulted in an underestimation of particle size or non-
24 detection of particles. Imaged examples of SP are shown in Fig. 4. Of the 3909
25 particles that were mapped, SP were the overall dominating type of particles with
26 82% of the total aerosol particles attributed to this group (Table 1). They were
27 observed over the whole size range between 15 nm and 800 nm in diameter with a
28 broad Aitken mode peaking at 64 nm accompanied by a less pronounced peak at 27
29 nm. The majority of SP (80%) appeared in the Aitken mode size region and below 80
30 nm in diameter (Table 1). In the accumulation mode size range, 18% of SP appeared
31 between 80 and 200 nm with a maximum at 106 nm in diameter and the remaining
32 2% of the SP were detected in diameter sizes (Table 1) > 200 nm (Fig. 5, upper panel).
33 We observed that 35% of the SP partly evaporated under the SEM electron beam but
34 retained their outer shape on the timescale of minutes. Also, at a higher magnification

1 using TEM, the same behavior was seen for 30% of the particles. We tentatively
2 assigned these particles to be ammonium (bi)sulfate particles. We were guided by the
3 results published by Heard and Wiffen (1969) and Bigg and Leck (2001b) where
4 particles with the same morphological features and instability under the electron
5 microscope were made up by ammonium sulfate, bisulfate or methane sulfonate
6 mixtures. The presence of ammonium sulfate or bisulfate particles would be
7 supported by the fact that ammonia has been reported to be the predominant base in
8 the remote marine troposphere (Söderlund, 1982) that undergoes primarily acid-base
9 reactions with non-seasalt H_2SO_4 , an oxidation product of biogenic dimethyl sulfide,
10 DMS (Quinn et al., 1987). Leck and Persson confirmed the presence of ammonia
11 bisulfate particles both along the marginal ice edge and over the inner parts of the
12 pack ice. Over remote marine locations at lower latitudes, Meszaros and Vissy (1974)
13 observed ammonium bisulfate concentrations up to 38% and on average 24%
14 contained the highest particle concentrations between 100 nm and 1 μm in diameter.
15 In the literature, chemical tests have also been used to identify ammonium and sulfate
16 in samples investigated by TEM (Bigg and Leck, 2001b). Such tests were not
17 implemented during this study since the use of chemicals would have added
18 additional mass onto the particles. This would have altered the size and the
19 morphology of the particles and hampered the investigation of the aerosol particles
20 with TEM and EDX spectroscopy.

21 The presence of biogenic nitrate as a counter ion to ammonium can be considered
22 rather unlikely since the formation of ammonium nitrate happens only after all sulfate
23 has been neutralized (Kuhn et al., 2010). Nitrate concentrations from impactor
24 measurements during ASCOS show nitrate values that are one order of magnitude
25 lower than sulfate concentrations at the same time, usually below 0.1 nmol m^{-3} (C.
26 *Leck pers. comm.*, 2015). Moreover, ammonium nitrate does not evaporate and is
27 stable under the electron beam (Rao et al., 1989). To minimize biases due to
28 evaporative losses and beam damage the ammonium sulfate particles were imaged as
29 quickly as possible. Fig. 6 (upper panel) shows the number size distribution of the
30 ammonium sulfate particles derived from the TEM images with a maximum at 172
31 nm in the accumulation mode.

32 The remaining 65% of the imaged particles (Fig. 5, upper panel) were stable under the
33 heat of the electron beam and showed no sign of evaporation or changes in
34 morphology. Some of those particles appeared as skeletal structures (Fig. 4B) that
35 collapsed and merged to an unstructured flat appearance after exposure times to the

1 electron beam significantly longer than the justified time for imaging of the particles.
2 None of the SP particles showed an apparently crystalline appearance that could be
3 attributed to sea salt or any other inorganic crystalline matter.

4

5 **3.3 Gel-like particles**

6 Aerosol particles classified as gel-like particles (GP) using SEM showed an
7 amorphous texture with an inhomogeneous distribution of pixel intensity. Their
8 diffuse structure and weak contrast to the Formvar-film suggested that these particles
9 predominantly contain light elements like C, H, N and O, which are typical
10 components of organic matter. The contrast between the particles and the Formvar-
11 film provides (indirect) information about the elemental composition of the aerosol
12 particle since the number of the detected secondary electrons increases with
13 increasing atomic number of the elements present in the aerosol particle (Zhou et al.,
14 2006) suggesting that the aerosol particles under investigation are built up by matter
15 of biological origin. The potential similarity in chemical composition between the GP
16 and the Formvar-film might have lead to an underestimation of the particle size which
17 resulted in the shift of the higher accumulation mode peak at 173 nm in TDMPS to
18 147 nm in the total number size distribution (Fig. 3).

19 GP appeared in the Aitken mode at diameters above 45 nm but were most frequently
20 observed in the accumulation mode with a maximum at 174 nm, covering all sizes up
21 to 800 nm (Fig. 5, middle panel). In total 11% of the 3909 particles that were imaged
22 were classified as GP of which 24% were observed in the Aitken mode > 45 nm,
23 | while 49% appeared in the accumulation mode between 80 and 200 nm, and 27%
24 were observed > 200 nm (Table 1).

25 Particles classified as GP were further evaluated with TEM. The higher resolution of
26 the TEM images revealed better insight into the morphology of the particles and the
27 | GP could be further divided into subgroups (see Fig. 2). Fourteen percent of the
28 particles consisted of a conglomeration of smaller spherical subunits that were welded
29 together and formed small chains or agglomerates (Fig. 7A, B). Those particles were
30 | named “*aggregate*” particles. Twenty nine percent of the gel particles appeared as
31 “*aggregate with film*” particles where “*aggregate*” particles were covered with a
32 diffuse and nearly electron-transparent film that partly obscured the underlying
33 subunits and produced a more smooth appearance compared to the bare “*aggregate*”

1 particles (Fig. 7 C, D and E). However, for the majority of GP, 57% showed a
2 “*mucus-like*” texture that was many times widely outspread on the Formvar-film
3 (Fig. 8 A, B), partly in long drawn-out structures (Fig. 8 C) or with small electron
4 dense inclusions (Fig. 8 D).

5 The individual subunits of “*aggregate*” particles and the dense spots in “*mucus-like*”
6 particles exhibit diameters between 11 nm and 109 nm with a maximum in number
7 size distribution at 39 nm and a smaller maximum at 28 nm. Fig. 9 compares the size
8 distributions of “*aggregate*” components from this study (red line) with those from
9 previous studies in the high Arctic and at lower latitudes (Leck and Bigg, 2005a;
10 2008; 2010). Similarity with previous studies outside and within the pack ice (Leck
11 and Bigg, 2005b; Orellana et al., 2011, same period as this study) strongly suggests
12 the presence of airborne marine gels. Entanglements, ionic or hydrophobic
13 interactions and/or hydrogen bonds stabilize the three-dimensional biopolymer
14 networks of the marine polymer gels, with electrostatic bonds involving Ca^{2+} or Mg^{2+}
15 ions being the most dominating (Verdugo, 2012; Orellana and Leck, 2015). In
16 seawater the observed size range of gel particles ranges from solvated nanogels (100-
17 200 nm; Bigg et al., 2004) that can further anneal into microgels (> 1000 nm) by
18 interpenetration and entanglement of neighboring nanogels or hydrophobic interaction.

19 Orellana and Verdugo (2003) have shown that changes in environmental factors like
20 enhanced UV-B radiation will avert gel particle formation or induce fragmentation of
21 existing gel particles in seawater (Orellana and Verdugo, 2003). Changes of pH and
22 temperature will lead to volume change of the gel polymer assemblies (Tanaka et al.,
23 1980; Orellana et al., 2011). The transport of marine gels from the ocean water into
24 the atmosphere is likely to result in an enhanced exposure of the particles to solar UV-
25 B radiation and might have lead to the fragmentation of airborne gel particles. In
26 cloud processing and the condensation of acidic gases onto the gel particles is
27 suggested to lead to a volume change of the gel particles similar to those observed in
28 seawater and produce gel particles with smaller diameters compared to the gel
29 particles observed in seawater (Leck and Bigg, 2005b; Orellana et al., 2011).

30 3.4 Halo particles

31 Besides SP and GP we observed particles with a halo-like appearance (halo particles,
32 HP) on the TEM grid where a relatively large central particle was surrounded by a
33 droplet ring structure of numerous smaller particles (for examples see Fig. 10).

1 Several authors (e.g., Farlow et al., 1977; Bigg, 1986; Bigg et Leck, 2001b) have
2 found that the formation of droplet ring structures from sulphuric acid containing
3 aerosol is a result of humidity, hydrophilicity of the collection surface and impact
4 velocity effects. Bigg and Leck (2001b) observed that a solution of sulfuric acid wets
5 out on a hydrophilic surface but retracts when humidity is reduced leaving behind
6 small droplets in a symmetrical ring. In our study, the sampling procedure led to a
7 drastic reduction in relative humidity from around 100% at ambient conditions to 20%
8 within the sampling manifold (see chapter 2.1.1). The aerosol was impacted onto a
9 surface with hydrophilic properties (TEM grid). We will assume that the HP
10 originally existed as one particle in the atmosphere that splashed out into the droplet
11 ring structure upon impaction onto the substrate.

12 HP comprised 7% of the total number of aerosol particles (Table 1) and were
13 observed at diameters above 75 nm and in the accumulation mode with maxima at
14 161 and 293 nm (Fig. 5, lower panel, left). The very weak contrast of the satellite
15 particles against the Formvar background (Fig. 3) probably shifted the particle
16 number size distribution towards smaller sizes to some extent.

17 Imaging with TEM allowed a more detailed investigation of the HP and revealed
18 three morphologically different types of the central particle. We observed central
19 particles in HP that consisted predominantly of skeletal structures or
20 "aggregate"/"aggregate with film" particles. Another types of particles was unstable
21 under the electron beam (Fig. 2). Central particles of skeletal structures or
22 "aggregate"/"aggregate with film" accounted for 19% and 22% of the HP. Examples
23 of both particle types are shown in Figs. 10(A) and 10(B). The majority of central
24 particles (59%), however, was unstable and seemed to partly evaporate during the
25 imaging process leaving more transparent structures behind, and was similar to the SP
26 described in chapter 3.2. We sized the central particles individually in order to
27 compare them with particles of similar morphology within SP or GP. The combined
28 number size distribution of the stable "aggregate", "aggregate with film" and
29 skeletal particles exhibited a maximum at 270 nm in diameter (Fig. 6(B) green line).
30 The number size distribution of unstable central particles showed a maximum at 171
31 nm (Fig. 6(B), red line). Unstable SP exhibited a maximum at nearly the same
32 diameter as unstable central particles, at 172 nm (Fig. 6(A)). The consistency in peak
33 position for unstable central particles and unstable SP suggested a similar chemical

1 | nature but different atmospheric processing that resulted in condensation of further
2 | chemical species and the formation of HP.

3 | The satellites (particulates or droplets) exhibited varying morphologies. Sometimes
4 | numerous small satellites surrounded the central particle in a symmetrical ring (Fig.
5 | 10(A) whereas in other cases the satellite droplets were larger but fewer (Fig. 10(B),
6 | (C)). In the literature three types of compounds have been described to form satellites
7 | when airborne aerosol particles impact on a collection substrate: sulfuric acid (Ayers,
8 | 1978; Ferek et al., 1983), ammonium sulfate and bisulfate (Bigg, 1980; Busek and
9 | Pósfai, 1999) and methane sulfonic acid, MSA, (Bigg et al., 1974). Sulfuric acid
10 | exhibits a distinctive morphology: a central particle surrounded by a droplet-halo of
11 | numerous smaller satellites. Neutralization of sulfuric acid by ammonium or a high
12 | content of methane sulfonic acid produces a halo of larger and fewer droplets (Bigg
13 | and Leck, 2001a). The morphology of the droplet-halos we observed in this study
14 | points towards the presence of sulfuric acid often in a mixture with ammonium sulfate
15 | or bisulfate and/or methane sulfonic acid. As discussed in section 3.2, these sulfur-
16 | containing components have not only been reported to be present over the Arctic pack
17 | ice area in summer (Bigg and Leck, 2001a) but also to frequently occur in the remote
18 | marine atmosphere (Barnard et al., 1994; Capaldo and Pandis, 1997; Kettle et al.,
19 | 1999). The observed number size distribution for all HP (Fig. 5, lower panel) is in
20 | agreement with results from the high Arctic reported by Hillamo et al. (2001), which
21 | observed the first maximum in sulfate containing aerosol particles at diameters > 80
22 | nm and in ammonium and MSA containing particles at diameters > 100 nm.

23 | **3.5 EDX measurements**

24 | To determine the elemental composition of the aerosol samples an EDX spectrometer
25 | coupled to TEM was used. EDX spectra of 103 aerosol particles were recorded in
26 | conjunction with the imaging process. Molecular dynamics studies on polysaccharides
27 | by Li et al. (2013) and Sun et al. (2014) have shown that not only the divalent ions
28 | Ca^{2+} and Mg^{2+} but also the monovalent ions Na^+ and K^+ can stabilize the three-
29 | dimensional biopolymer gel networks. Inspired by these results, we focused on the
30 | detection of the alkali ions Na^+ and K^+ and the divalent ions Ca^{2+} and Mg^{2+} in the gel-
31 | type particles. In the following, we will refer to Na^+ and K^+ as Na^+/K^+ and Ca^{2+} and
32 | Mg^{2+} as $\text{Ca}^{2+}/\text{Mg}^{2+}$.

1 The analysis revealed the following characteristics: Na^+/K^+ was detected in 91% of
2 the SP. Thirteen percent of these particles contained exclusively Na^+/K^+ whereas 78%
3 contained both types of metal ions, Na^+/K^+ and $\text{Ca}^{2+}/\text{Mg}^{2+}$ with the latter only in
4 minor quantities (Fig. 11(A)). Examples of EDX spectra for the different types of
5 particles are shown in Fig. S1. The “aggregate” particles contained exclusively
6 Na^+/K^+ in 20% of the particles and predominantly Na^+/K^+ and minor contents of
7 $\text{Ca}^{2+}/\text{Mg}^{2+}$ in 80% of the particles (Fig. 11(B)). For the particle types “aggregate with
8 film” and “mucus-like” particles, however, a clear dominance of only $\text{Ca}^{2+}/\text{Mg}^{2+}$ was
9 detected. Eighty-four percent of “aggregate with film” particles contained $\text{Ca}^{2+}/\text{Mg}^{2+}$
10 as the dominating type of ions. Seventeen percent of the “aggregate with film”
11 particles contained exclusively $\text{Ca}^{2+}/\text{Mg}^{2+}$ and 67% of the “aggregate with film”
12 particles contained $\text{Ca}^{2+}/\text{Mg}^{2+}$ that were accompanied by minor contents of Na^+/K^+
13 (Fig. 11(C)). “Mucus-like” particles also showed a clear dominance of $\text{Ca}^{2+}/\text{Mg}^{2+}$.
14 Eleven percent of “mucus-like” particles contained exclusively $\text{Ca}^{2+}/\text{Mg}^{2+}$ and 86%
15 contained $\text{Ca}^{2+}/\text{Mg}^{2+}$ that was accompanied by minor contents of of Na^+/K^+ (Fig. 11(D)).
16 In summary, we observed a gradual transition from particles with a dominating
17 content of Na^+/K^+ to particles with a dominating content of $\text{Ca}^{2+}/\text{Mg}^{2+}$ moving from
18 SP over “aggregate” particles and “aggregate with film” particles to “mucus-like”
19 particles. Therefore, we hypothesise a connection between the morphology of the
20 particles and the respective dominating crosslinking ion within the polymer 3-
21 dimensional network of the marine gels. Li et al. (2013) compared polysaccharides
22 with 3 and 4 repetition units of molecular weights of 1.9 kDa and 2.5 kDa,
23 respectively as representations for organic matter in seawater (Verdugo, 2004). Their
24 results showed that the assembly of the longer polysaccharide chains seems to be
25 accelerated in the presence of Ca^{2+} whereas the presence of Na^+ has a positive effect
26 on the assembly of shorter polysaccharide chains. Considering the observed
27 morphology of the aerosol particles that are built up by marine gel matter, a high
28 content of $\text{Ca}^{2+}/\text{Mg}^{2+}$ could facilitate the formation of fluffy and less compact
29 “mucus-like” gel matter. The presence of Na^+/K^+ , however, favored a more compact
30 structure of type “aggregate” and SP.

31 Halo particles with a center of gel or fraction of a gel showed a high content of
32 Na^+/K^+ : Fifty percent of the particles contained those metals exclusively whereas
33 another 25% contained mainly Na^+/K^+ with smaller amounts of $\text{Ca}^{2+}/\text{Mg}^{2+}$ (Fig. 12).
34 The high content of alkali metal ions in those particles suggested that they originated

1 from SP or fragmented “*aggregate*” particles, which were exposed to processes that
2 lead to condensational growth of the original gel particles.

3

4 **4 Summary and conclusions**

5 Aerosol particles collected in the summer high Arctic north of 80° were individually
6 and objectively investigated with electron microscopy and subsequent image mapping.
7 This enabled a division of the aerosol particles into three size resolved gross
8 | morphological groups: single particles (SP), gel particles (GP) and halo particles (HP).
9 Single particles (SP) dominated the aerosol population in terms of numbers and made
10 up 82% of all particles; they were observed over the whole sub-micrometer size range
11 and clearly dominated the Aitken mode. The majority of SP (65%) was stable under
12 the electron microscope and showed no signs of evaporation or morphological
13 changes during imaging. These particles with refractory properties appeared over the
14 whole size range of particles observed whereas the remaining 35% of SP appeared to
15 be heat unstable, evaporated partly and were predominantly observed in the
16 accumulation mode. GP were observed at diameters > 45 nm predominantly in the
17 accumulation mode with a maximum at 154 nm and contributed 11% to the total
18 particle number. The GP exhibited various morphological features and appeared as
19 | “*aggregate*” particles (14%) and as “*aggregate with film*” particles (29%), but the
20 | majority (59%) was made up by “*mucus-like*” particles. Seventy percent of the GP in
21 our study appeared to be smaller than 100 nm in diameter, and 90% were smaller than
22 200 nm.

23 HP appeared mainly in the accumulation mode at diameters > 60 nm with a maximum
24 | at 161 nm, that contributed up to 7% to the total particle number mapped. The
25 | majority of HP consisted of heat unstable particles, probably ammonium bisulfate
26 | (59% of all particles), that were internally mixed with sulfur containing compounds
27 | (sulfuric acid, ammonium bisulfate, methane sulfonic acid). The remaining fraction
28 | was made up by “*aggregate*” particles (19%) and decomposed or fragmented gel
29 | matter (22%) internally mixed with sulfur containing compounds.

30 Electron dispersive X-ray (EDX) spectroscopy revealed a gradual transition in the
31 content of Na^+/K and $\text{Ca}^{2+}/\text{Mg}^{2+}$ between different particle morphologies. SP and
32 | “*aggregate*” particles preferentially contained Na^+/K^+ whereas “*aggregate with film*”
33 | particles and “*mucus-like*” particles contained mainly $\text{Ca}^{2+}/\text{Mg}^{2+}$ with minor contents

1 of Na^+/K^+ . Supported by model studies (e.g. Li et al., 2013; Sun et al., 2014), we
2 hypothesize a correlation between particle morphology and the presence of the ions
3 Na^+/K^+ and/or $\text{Ca}^{2+}/\text{Mg}^{2+}$. The prevalence of $\text{Ca}^{2+}/\text{Mg}^{2+}$ facilitates the formation of
4 large organic assemblies of GP type whereas a lack of $\text{Ca}^{2+}/\text{Mg}^{2+}$ and a prevalence of
5 Na^+/K^+ prohibit the formation of large assemblies and result in smaller entities of SP
6 type.

7 Insufficient knowledge of the size resolved aerosol composition and especially the
8 role of organic compounds including their morphology and state of mixture had
9 hampered a detailed understanding of the processes that lead to the activation of the
10 high Arctic aerosol particles and their role in the formation of cloud droplets (Leck
11 and Svensson, 2015; Martin et al., 2011; Zhou et al., 2001; Leck et al., 2002). One
12 evident outcome from this study is that the aerosol particles that would be activated
13 into cloud droplets over the Arctic pack ice areas cannot be seen as simply inorganic
14 salts. None of the aerosol particles showed an apparent cubic or otherwise crystalline
15 appearance that could be attributed to sea salt particles. The results from this study
16 clearly show that organic marine gel matter significantly contributes to the particle
17 number concentration over the whole sub-micrometer size range, especially at
18 diameters below 60 nm.

19 A parallel study conducted during the ASCOS campaign (Orellana et al., 2011)
20 demonstrated that airborne aerosol particles contain hydrophobic moieties on their
21 surface that play an important role for gel formation (Maitra et al., 2001) and increase
22 the rate of gel assembly (Ding et al., 2008). The interaction of the hydrophilic and
23 hydrophobic entities on the structure of the polymer gels likely will influence the
24 water vapor pressure and decrease the surface tension of the cloud droplets to be
25 formed (Leck and Svensson, 2015; Ovadnevaite et al., 2011).

26 Water-soluble particles like ammonium sulfate were present mainly in the
27 accumulation mode at diameters above 100 nm. Growth of the sub-Aitken particles
28 probably resulted from deposition of acids/organic vapors on polymer gel particles
29 and produced HP or sulfur containing particles with hygroscopic properties typical for
30 a gel nucleus covered by a sulfate-methane sulfonate-ammonium complex. At the
31 same time the fragmentation of larger particles is capable of adding numbers into the
32 Aitken mode (Leck and Bigg, 1999; 2010; Karl et al., 2013). Orellana and Verdugo
33 (2003) and Orellana et al. (2011) observed the sensitivity of marine gels to changes in
34 the physicochemical environment (pH and T) and the fragmentation of gel matter into

1 smaller entities as a result to UV radiation exposure. Acidic compounds typically
2 found in the marine atmosphere like sulfuric acid and dimethyl sulfide (DMS)
3 induced volume collapse of the swollen hydrated polymer gel network into a
4 condensed and more compact form (Tanaka et al., 1980; Leck and Bigg, 2010;
5 Orellana et al., 2011). Condensation of sulfur acidic compounds and in-cloud
6 processing of the marine gels in the atmosphere during their passage over the pack-ice
7 and continuous exposure to UV radiation due to the length of the polar day in summer
8 could produce smaller sized fragments of marine gels similar to the spherical subunits
9 observed in “aggregate”/”aggregate with film” particles and the dense inclusions in
10 “mucus-like” particles. Since SP showed a maximum in number concentration in the
11 same size range (i.e., 27 nm), it cannot be excluded that fragmentation of gel matter or
12 pH induced collapse of the gels lead to the formation of smaller entities that provided
13 a mechanism to produce SP and add particle numbers to the Aitken mode.

14 In hope of enhancing our understanding on CCN properties promoting/suppressing
15 cloud droplet formation over the pack ice area in summer, and at the same time meet
16 the demand for observational data for the evaluation of climate models, this study has
17 presented critical size resolved data on particle morphology, chemical composition
18 and state of mixture based on the analysis of individual particles.

19

20

21

1 **Acknowledgements**

2 This work is part of the ASCOS (Arctic Summer Cloud Ocean Study). ASCOS was
3 an IPY project under the AICIA-IPY umbrella and an endorsed SOLAS project.
4 ASCOS was made possible by funding from the Knut and Alice Wallenberg
5 Foundation, the DAMOCLES Integrated Research Project from the European Union
6 6th Framework Program and the Swedish National Research Council (VR). The
7 Swedish Polar Research Secretariat provided access to the icebreaker Oden and
8 logistical support. The authors thank A. Held for collecting the aerosol particles
9 during ASCOS, and A. Öhrström and C. Rauschenberg for their help with sample
10 imaging / EDX measurements.

11

1 **References**

2 Albrecht, B.: Aerosols, cloud microphysics and fractional cloudiness, *Nature*, 367,
3 445-447, 1994.

4 Allen, T.: *Particle Size Measurement: Volume 1*, Chapman & Hall, London, 1997.

5 Ayers, G. P.: Quantitative determination of sulfate in individual aerosol particles,
6 *Atmos. Environ.* 12, 1613-1621, 1978.

7 Barnard, W. R., Andreae, M. O. and Iverson, R. L.: Dimethylsulfide and *Phaeocystis*
8 *pouchetii* in the southeastern Bering Sea, *Cont. shelf Res.*, 3, 103-113, 1984.

9 Bates, T. S., Cline, J. D., Gammon, R. H., and Kelly-Hansen, S. R.: Regional and
10 seasonal variations in the flux of oceanic dimethylsulfide to the atmosphere, *J.*
11 *Geophys. Res.*, 92(C3), 2930-2938, doi: 10.1029/JC092iC03p02930, 1987.

12 Bigg, E. K. and Leck, C.: Cloud-active particles over the central Arctic Ocean, *J.*
13 *Geophys. Res.*, 106, 32155-32166, doi: 10.1029/1999JD901152, 2001a.

14 Bigg, E.K. and Leck, C.: Properties of the aerosol over the central Arctic Ocean, *J.*
15 *Geophys. Res.*, 106:D23, 32101-32109, doi: 10.1029/1999JD901136, 2001b.

16 Bigg, E. K., and Leck, C.: The composition of fragments of bubbles bursting at the
17 ocean surface, *J. Geophys. Res.* 113(D11209), doi 10.1029/2007JD009078, 2008.

18 Bigg, E. K., Ono, A. and Williams, J. A.: Chemical tests for individual submicron
19 aerosol particles, *Atmos. Environ.*, 8, 1-13, 1974.

20 Bigg, E. K., Leck, C. and Nilsson, E. D.: Sudden changes in arctic atmospheric
21 aerosol concentrations during summer and autumn, *Tellus B*, 48, 254-271,
22 doi: 10.1034/j.1600-0889.1996.t01-1-00009.x, 1996.

23 Bigg, E. K., Leck, C. and Tranvik, L.: Particulates of the surface microlayer of open
24 water in the central Arctic Ocean in summer, *Mar. Chem.*, 91, 131-141, 2004.

25 Busek, P. R. and Pósfai, M.: Airborne minerals and related aerosol particles: effects
26 on climate and the environment, *Proc. Natl. Acad. Sci. USA*, 96, 3372-3379, 1999.

27 Capaldo, K. P. and Pandis, S. N.: Dimethylsulfide chemistry in the remote marine
28 atmosphere: Evaluation and sensitivity analysis of available mechanisms, *J. Geophys.*
29 *Res.*, 102, 23251-23267, 1997.

30 Carslaw, K. S., Lee, A., Reddington, C. L., Pringle, K. J., Rap, A., Forster, P. M.,
31 Mann, G. W., Spracklen, D. V., Woodhouse, M. T., Regayre, L. A., and Pierce, J. R.:

1 Large contribution of natural aerosols to uncertainty in indirect forcing, *Nature*, 503,
2 67-71, doi: 10.1038/nature12674, 2013.

3 Chi J. W., Li, W. J., Zhang D. Z., Lin Y. T., Shen X. J., Sun J. Y., Chen J. M., Zhang
4 X. Y., Zhang Y. M., and Wang W. X.: Sea salt aerosols as a reactive surface for
5 inorganic and organic acidic gases in the arctic troposphere, *Atmos. Chem. Phys.*
6 *Discus.*, 15, 16715-16745, doi: 10.5194/acpd-15-16715-2015, 2015.

7 Chin, W.-C., Orellana, M. V. and Verdugo, P.: Spontaneous assembly of marine
8 dissolved organic matter into polymer gels, *Nature*, 391, 568-572, 1998.

9 Covert, D. S., Wiedensohler, A., Aalto, P., Heintzenberg, J., McMurry, P. H., and
10 Leck, C.: Aerosol number size distributions from 3 to 500 nm diameter in the arctic
11 marine boundary layer during summer and autumn, *Tellus*, 48B, 197-212, 1996.

12 Decho, A. W.: Microbial exopolymer secretions in ocean environments – their role(s)
13 in food webs and marine processes, *Oceanogr. Mar. Biol. Ann. Rev.*, 28, 73-153,
14 1990.

15 Ding, Y.-X., Chin, W.-C., Rodriguez, A., Hung, C.-C., Santschi, P. H. and Verdugo,
16 P.: Amphiphilic exopolymers from *Sagittula stellata* induce DOM self-assembly and
17 formation of marine microgels, *Mar. Chem.*, 112, 11-19, 2008.

18 Dixkens, J. and Fissan, H.: Development of an Electrostatic Precipitator for Off-Line
19 Particle Analysis, *Aerosol. Sci. Tech.*, 30, 438–453, 1999.

20 Douglas, T., and Sturm, M.: Arctic haze, mercury and the chemical composition of
21 snow across northwestern Alaska, *Atmos. Environm.* 38, 805–820, 2004.

22 Egerton, R. F.: *Physical Principles of Electron Microscopy*, Springer, New York,
23 USA, 2008.

24 Engvall, A.-C., Krejci, R., Ström, J., Treffeisen, R., Scheele, R., Hermansen, O. and
25 Paatero, J.: Changes in aerosol properties during spring-summer period in the Arctic
26 troposphere, *Atmos. Chem. Phys.* 8, 445-462, doi:10.5194/acp-8-445-2008, 2008.

27 Ferek, R. J., Lazrus, A. L. and Winchester, W.: Electron microscopy of acidic
28 aerosols collected over the northeastern United States, *Atmos. Environ.*, 17:8, 1545-
29 1561, 1983.

30 Fitzgerald, J. W.: Marine aerosols: a review, *Atmos. Environ.*, 25A:3/4, 533-545,
31 1991.

1 Forster, P., Ramaswamy, V., Artaxo, P., Berntsen, T., Betts, R., Fa-
2 haywood, J., Lean, J., Lowe, D. C., Myhre, G., Nganga, J., Prinn, R., Raga, G.,
3 Schulz, M., and Van Dorland, R.: Changes in atmospheric constituents and in
4 radiative forcing, in: Climate Change 2007: The Physical Science Basis. Contribution
5 of Working Group I to the Fourth Assessment Report of the Intergovernmental Panel
6 on Climate Change, edited by: Solomon, S., Qin, D., Manning, M., Chen, Z.,
7 Marquis, M., Averyt, K. B., Tignor, M., and Miller, H. L., Cambridge University
8 Press, Cambridge, United Kingdom and New York, NY, USA, 2007.

9 Geng, H., Ryu, J., Jung, H.-J., Chung, H., Ahn, K.-H. and Ro, C.-U.: Single-Particle
10 Characterization of Summertime Arctic Aerosols Collected at Ny-Alesund, Svalbard,
11 Environmental Science & Technology, 44(7), 2348-2353, 2010.

12 Hamacher-Barth, E., Jansson, K., and Leck, C.: A method for sizing submicrometer
13 particles in air collected on Formvar films and imaged by scanning electron
14 microscopy, Atmos. Meas. Tech., 6, 3459-3475, 2013, doi: 10.5194/amt-6-3459-
15 2013.

16 Hara, K., Yamagata, S., Yamanouchi, T., K. Sato, K., Herber, A., Iwasaka, Y.,
17 Nagatani, M. and Nakata, H.: Mixing states of individual aerosol particles in spring
18 Arctic troposphere during ASTAR 2000 campaign, Journal of Geophysical Research-
19 Atmospheres, 108(D7), 4209, 2003.

20 Heard, M. J. and Wiffen, R. D.: Electron microscopy of natural aerosols and the
21 identification of particulate ammonium sulfate, Atm. Environm., 3:3, 337-340, 1969.

22 Heintzenberg, J. and Leck, C.: Seasonal variations of the atmospheric aerosol near the
23 top of the marine boundary layer over Spitsbergen related to the Arctic sulfur cycle,
24 Tellus, 46B, 52-67, 1994.

25 Heintzenberg, J., and Leck, C.: The summer aerosol in the central Arctic 1991-2008:
26 did it change or not?, Atmos. Chem. Phys., 12, 3969-3983, 2012.

27 Heintzenberg, J., Leck, C., Birmili, W., Wehner, B., Tjernström, M. and
28 Wiedensohler, A.: Aerosol number-size distributions during clear and fog periods in
29 the summer high Arctic: 1991, 1996 and 2001, Tellus, 58B, 41-50, doi:
30 10.1111/j.1600-0889.2005.00171.x, 2006.

1 Heintzenberg, J., Leck, C. and Tunved, P.: Potential source regions and processes in
2 the summer Arctic, *Atmos. Chem. Phys.*, 15, 6487-6502, doi:10.5194/acp-15-6487-
3 2015, 2015.

4 Held, A., Brooks, I. M., Leck, C., and Tjernström, M.: On the potential contribution
5 of open lead particle emissions to the central Arctic aerosol concentration, *Atmos.*
6 *Chem. Phys.*, 11(7), 3093-3105, 2011a.

7 Held, A., Orsini, D. A., Vaattovaara, P., Tjernström, M., and Leck, C.: Near-surface
8 profiles of aerosol number concentration and temperature over the Arctic Ocean,
9 *Atmos. Meas. Tech.*, 4, 1603–1616, 2011b.

10 Hillamo, R., Kerminen, V.-M., Aurela, M., Mäkelä, T., Maenhaut, W., and Leck, C.:
11 Modal structure of chemical mass size distribution in the high Arctic aerosol, *J.*
12 *Geophys. Res.*, 106(D21), 27555-27571, doi: 10.1029/2001JD001119, 2001.

13 Hinds, W.: *Aerosol Technology*, 2nd ed., John Wiley & Sons, New York, 1999.

14 Hoppel, W. A., Frick, G. M., and Larson, R. E.: Effect of nonprecipitating clouds on
15 the aerosol size distribution in the marine boundary layer, *Geophys. Res. Lett.*, 13,
16 125-128, 1986.

17 Karl, M., Leck, C., Coz, E. and Heintzenberg, J.: Marine nanogels as a source of
18 atmospheric nanoparticles in the high Arctic, *Geophys. Res. Lett.*, 40:14, 3738-3743,
19 2013.

20 Kettle, A. J., Andreae, M. O., Amouroux, D., Andreae, T. W., Bates, T. S.,
21 Berresheim, H., Bingemer, H., Boniforti, R., Curran, M. A. J., DiTullio, G. R., Helas,
22 G., Jones, G. B., Keller, M. D., Kiene, R. P., Leck, C., Levasseur, M., Maspero, M.,
23 Matrai, P., McTaggat, A. R., Mihalopoulos, N., Nguyen, B. C., Novo, A., Putaud, J.
24 P., Rapsomanikis, S., Roberts, G., Schebeske, G., Sharma, S., Simo, R., Staubies, R.,
25 Turner, S., Uher, G.: A global database of sea surface dimethylsulphide (DMS)
26 measurements and a simple model to predict sea surface DMS as a function of
27 latitude, longitude and month, *Global Biogeochem. Cy.* 13, 399-444, 1999.

28 Korhonen, H., Carslaw, K. S., Spracklen, D. V., Ridley, D. A. and Ström, J.: A global
29 model study of processes controlling aerosol size distributions in the Arctic spring and
30 summer, *J. Geophys. Res.*, 113, D08211-D08211, doi: 10.1029/2007JD009114, 2008.

1 Krembs, C., Eicken, H., Junge, K. and Deming, J. W.: High concentrations of
2 exopolymeric substances in Arctic winter sea ice: implications for the polar ocean
3 carbon cycle and cryoprotection of diatoms, *Deep Sea Res. I*, 49, 2163-2181, 2002.

4 Kuhn, T., Damoah, R., Bacak, A., and Sloan, J. J.: Characterising aerosol transport
5 into the Canadian High Arctic using aerosol mass spectrometry and Lagrangian
6 modelling, *Atmos. Chem. Phys.*, 10(21), 10489-10505, doi:10.5194/acp-10-10489-
7 2010, 2010.

8 Lannefors, H., Heintzenberg, J., and Hansson, H.-C.: A comprehensive study of
9 physical and chemical parameters of the Arctic summer aerosol; results from the
10 Swedish expedition Ymer-80, *Tellus*, 35B, 40-54, 1983.

11 Leck, C. and Svensson, E.: Importance of aerosol composition and mixing state for
12 cloud droplet activation over the Arctic pack ice in summer, *Atmos. Chem. Phys.*,
13 15(5), 2545-2568, doi:10.5194/acp-15-2545-2015, 2015.

14 Leck, C. and Bigg, E. K.: Evolution of marine aerosol – a new perspective, *Geophys.*
15 *Res. Lett.*, 32, L19803, doi: 10.1029/2005GL023651, 2005a.

16 Leck, C. and Bigg, E. K.: Biogenic particles in the surface microlayer and overlaying
17 atmosphere in the central Arctic Ocean during summer, *Tellus B*, 57, 305-316, doi:
18 10.1111/j.1600-0889.2005.00148.x, 2005b.

19 Leck, C. and Bigg, E. K.: Comparison of sources and nature of the tropical aerosol
20 with the summer high Arctic aerosol, *Tellus*, 60B, 118-126, 2008.

21 Leck, C. and Bigg, E. K.: New particle formation of marine biological origin, *Aerosol*
22 *Sci. Tech.*, 44(7), 570-577, 2010.

23 Leck, C. and Nilsson, D. E.: A pseudo-Lagrangian study of the sulfur budget in the
24 remote Arctic marine boundary layer, *Tellus*, 54B, 213-230, 2002.

25 Leck, C., Bigg, E. K., Covert, D. S., Heintzenberg, J., Maenhaut, W., Nilsson, E. D.,
26 and Wiedensohler, A.: Overview of the atmospheric research program during the
27 International Arctic Ocean Expedition 1991 (IAOE-91) and its scientific results,
28 *Tellus*, 48B, 136-155, 1996.

29 Leck, C., Nilsson, E. D., Bigg, E. K. and Bäcklin, L.: The atmospheric program of the
30 Arctic Ocean Expedition 1996 (AOE-96): An overview of scientific goals,
31 experimental approach, and instruments, *J. Geophys. Res.*, 106, 32051-32067, 2001.

1 Leck, C., Tjernström, M., Matrai, P., Swietlicki, E. and Bigg, E. K.: Can marine
2 micro-organisms influence melting of the Arctic pack ice?, EOS, 85, 25-36, 2004.

3 Leck, C., Gao, Q., Mashayekhy Rad, F. and Nilsson, U.: Size resolved atmospheric
4 particulate polysaccharides in the high summer Arctic, *Atmos. Chem. Phys.*, 13,
5 12573-12588, doi: 10.5194/acp-13-12573-2013, 2013.

6 Leck, C., Norman, M., Bigg, E. K., and Hillamo, R.: Chemical composition and
7 sources of the high Arctic aerosol relevant for cloud formation, *J. Geophys. Res.*
8 107(D12), 4135-4153, doi: 10.1029/2001JD001463, 2002.

9 Lee, L. A., Pringle, K. J., Reddington, C. L., Mann, G. M., Stier, P., Spracklen, D. V.,
10 Pierce, J. R. and Carslow, K. D.: The magnitude and causes of uncertainty in global
11 model simulations of cloud condensation nuclei, *Atmos. Chem. Phys.* 13, 8879-8914,
12 2013.

13 Li, X., Leck, C., Sun, L., Hede, T., Tu, Y., and Ågren, H.: Cross-linked
14 polysaccharide assemblies in marine gels: an atomistic simulation, *J. Phys. Chem.*
15 Lett., 4, 2637-2642, doi: 10.1021/jz401276r, 2013.

16 Lohmann, U. and Leck, C.: Importance of submicron surface-active organic aerosols
17 for pristine Arctic clouds, *Tellus*, 57B, 261-268, 2005.

18 Maitra, U., Mukhopadhyay, S., Sarkar, A., Rao, P., Indi, S. S.: Hydrophobic pockets in
19 a nonpolymeric aqueous gel: observation of such a gelation process by color change,
20 *Angew. Chem. Int. ed.* 40, 2281-2283, 2001.

21 Mancuso-Nichols, C. A., Guezennec, J. and Bowman, J. P.: Bacterial
22 exopolysaccharides from extreme marine environments, with special consideration of
23 the Southern Ocean, sea ice and hydrothermal vents: a review, *J. Appl. Microbiol.*, 96,
24 1057-1066, 2005.

25 Mann, G. W., Carslaw, K. S., Reddington, C. L., Pringle, K. J., Schulz, M., Asmi, A.,
26 Spracklen, D. V., Ridley, D. A., Woodhouse, M. T., Lee, L. A., Zhang, K., Ghan, S.
27 J., Easter, R. C., Liu, X., Stier, P., Lee, Y. H., Adams, P. J., Tost, H., Lelieveld, J.,
28 Bauer, S. E., Tsigaridis, K., van Noije, T. P. C., Strunk, A., Vignati, E., Bellouin, N.,
29 Dalvi, M., Johnson, C. E., Bergman, T., Kokkola, H., von Salzen, K., Yu, F., Luo, G.,
30 Petzold, A., Heintzenberg, J., Clarke, A., Ogren, J. A., Gras, J., Baltensperger, U.,
31 Kaminski, U., Jennings, S. G., O'Dowd, C. D., Harrison, R. M., Beddows, D. C. S.,
32 Kulmala, M., Viisanen, Y., Ulevicius, V., Mihalopoulos, N., Zdimal, V., Fiebig, M.,

1 Hansson, H.-C., E. Swietlicki, and Henzing, J. S.: Intercomparison and evaluation of
2 global aerosol microphysical properties among AeroCom models of a range of
3 complexity, *Atmos. Chem. Phys.*, 14, 4679-4713, doi: 10.5194/acp-14-4679-2014,
4 2014.

5 Martin, M., Chang, R. Y.-W., Sierau, B., Sjogren, S., Swietlicki, E., Abbatt, J. P. D.,
6 Leck, C. and Lohmann, U.: Cloud condensation nuclei closure study on summer arctic
7 aerosol, *Atmos. Chem. Phys.*, 11, 11335-11350, doi: 10.5194/acp-11-11335-2011,
8 2011.

9 Mauritzen, T., Sedlar, J., Tjernström, M., Leck, C., Martin, M., Shupe, M., Sjogren,
10 S., Sierau, B., Persson, P. O. G., Brooks, I. M., and Swietlicki, E.: An Arctic CCN-
11 limited cloud-aerosol regime, *Atmos. Chem. Phys.* 11, 165-173, doi: 10.5194/acp-11-
12 165-2011, 2011.

13 Michael, J. R., Joy, D. C., and Griffin, B. J.: Use of sample bias voltage for low-
14 energy high-resolution imaging in the SEM, *Microsc. Microanal.*, 16 (Suppl. 2), 614-
15 615, doi: 10.1017/S1431927610055315, 2010.

16 Nilsson, D. E. and Leck, C.: A pseudo-Lagrangian study of the sulfur budget in the
17 remote Arctic marine boundary layer, *Tellus*, 54(B), 213-230, 2002.

18 Okada, K.: Nature of individual hygroscopic particles in the urban atmosphere, *J.*
19 *Met. Soc. Jpn.*, 61(5), 727-735, 1983.

20 Orellana, M. V., Lessard, E. J., Dycus, E., Chin, W. C., Foy, M. S. and Verdugo, P.:
21 Tracing the source and the fate of biopolymers in seawater: application of an
22 immunological technique, *Mar. Chem.*, 83, 89-99, 2003.

23 Orellana, M. V., and Verdugo, P.: Ultraviolet radiation blocks the organic carbon
24 exchange between the dissolved phase and the gel phase in the ocean, *Limnol.*
25 *Oceanogr.*, 48, 1618-1623, 2003.

26 Orellana, M. V., Petersen, T. W., Diercks, A. H., Donohoe, S., Verdugo, P., van den
27 Engh, E.: Marine microgels: optical and proteomic fingerprints, *Mar. Chem.*, 105,
28 229-239, 2007.

29 Orellana, M. V., Matrai, P. A., Leck, C., Rauschenberg, C. D., Lee, A. M., and Coz,
30 E.: Marine microgels as a source of cloud condensation nuclei in the high Arctic,
31 *PNAS*, 108, 13612-13617, doi: 10.1073/pnas.1102457108, 2011.

1 Orellana, M. V., Pang, W. L., Durand, P. M., Whitehead, K., Baliga, N. S.: A role for
2 programmed cell death in the microbial loop, PLoS One 8, e62595, 2013.

3 Ovadnevaite, J., Ceburnis, D., Martucci, G., Bialek, J., Monahan, C., Rinaldi, M.,
4 Facchini, M. C., Berresheim, H., Worsnop, D. R., and O'Dowd, C.: Primary marine
5 organic aerosol: A dichotomy of low hygroscopicity and high CCN activity, Geophys.
6 Res. Lett., 38, L21806, doi: 10.1029/2011GL048869, 2011.

7 Parungo, F. P., Nagamoto, C. T., Rosinski, J. and Haagenson, P. L.: Marine aerosol in
8 Pacific upwelling regions, J. Aerosol Sci., 18, 277-290, 1987.

9 Parungo, F. P., Nagamoto, C. T., Rosinski, J. and Haagenson, P. L.: A study of
10 marine aerosols over the Pacific Ocean, J. Atmos. Chem., 4, 199-226, 1986.

11 Penner, J. E., Andreae, M., Annegarn, H., Barrie, L., Feichter, J., Hegg, D.,
12 Jayaraman, A., Leaitch, R., Murphy, D., Nganga, J., and Pitar, G.: Aerosols, their
13 Direct and Indirect Effects, in: Climate Change 2001: The Scientific Basis,
14 Contribution of Working Group I to the Third Assessment Report of the Intergovern-
15 mental Panel on Climate Change, edited by: Houghton, J. T., Ding, Y., Griggs, D. J.,
16 Noguer, M., van der Linden, P. J., Dai, X., Maskell, K., and Johnson, C. A.,
17 Cambridge University Press, Cambridge, United Kingdom and New York, NY, USA,
18 2001.

19 Quinn, P. K., Charlson, R. J. and Zoller, W. H.: Ammonia, the dominant base in the
20 remote marine troposphere: a review, Tellus, 39B, 413-425, 1987.

21 Rao, K. V. R., Hariharan, P. L., Jagannathan, K., Yoganarasimhan, S. R.: Scanning
22 electron microscopy of ammonium nitrate prills in relation to their application in
23 ammonium nitrate-fuel oil systems, Fuel, 68:9, 1118-1122, doi:10.1016/0016-
24 2361(89)90181-6, 1989.

25 Rocha, S., Krastev, R., Thünemann, A. F., Pereira, M. C., Möhwald, H., and
26 Bezesinski, G.: Adsorption of amyloid β -peptide at polymer surfaces: a neutron
27 reflectivity study, Chem. Phys. Chem., 6, 2527-2534, doi: 10.1002/cpc.200500158,
28 2005.

29 Schimel, D., Alves, D., Enting, I., Heimann, M., Joos, F., Raynaud, D., Wigley, T.,
30 Prather, M., Derwent, R., Ehhalt, D., Fraser, P., Sanhueza, E., Zhou, X., Jonas, P.,
31 Charlson, R., Rodhe, H., Sadasivan, S., Shine, K. P., Fouquart, Y., Ramaswamy, V.,
32 Solomon, S., Srinivasan, J., Albritton, D., Isaksen, I., Lal, M., and Wuebbles, D.:

1 Radiative forcing of climate change, in: Climate Change 1996, Contribution of
2 Working Group I to the 2nd Assessment Report of the Intergovernmental Panel on
3 Climate Change, edited by: Houghton, J. T., Meira Filho, L. G., Callander, B. A.,
4 Harris, N., Kattenberg, A., and Maskell, K., Cambridge University Press, Cambridge,
5 United Kingdom and New York, NY, USA, 1996.

6 Shaw, G. E.: Biocontrolled thermostasis involving the sulfur cycle, *Clim. Change*, 5,
7 297-303, 1983.

8 Shaw, G. E.: Microparticle size spectrum of Arctic haze, *Geophys. Res. Lett.*, 11:5,
9 409-412, 1984.

10 Shaw, G. E.: The arctic haze phenomenon, *Bull. Am. Met. Soc.*, 76:12, 2403-2413,
11 1995.

12 Solomon, S., Quin, D., Manning, M., Chen, Z., Marquis, M., Averyt, K. B., Tignor,
13 M., and Miller, H. L.: Climate change 2007: The physical science basis, Cambridge
14 University Press, 996 pp., 2007.

15 Söderlund, R.: Ammonia in the atmosphere, PhD dissertation, University of
16 Stockholm, Stockholm, Sweden, 1982.

17 Stevens, S. M., Jansson, K., Xiao, C., Asahina, S., Klingstedt, M., Grüner, D.,
18 Sakamoto, Y., Keiichi, M., Cubillas, P., Brent, R., Han, L., Che, S., Ryoo, R., Zhao,
19 D., Anderson, M., Schüth, F., and Terasaki, O.: An Appraisal of High Resolution
20 Scanning Electron Microscopy to Porous Material, *JEOL news*, 44:1, 17-22, 2009.

21 Stohl, A.: Characteristics of atmospheric transport into the Arctic troposphere, *J.
22 Geophys. Res.*, 111, D11306, doi:10.1029/2005JD006888, 2006.

23 Stolzenburg, M. R.: An ultrafine aerosol size distribution measuring system, Ph.D.
24 Thesis, University of Minnesota, Minneapolis, USA, 1988.

25 Ström, J., Umegård, K., Tørseth, K., Tunved, P., Hansson, H.-C., Holmén, K.,
26 Wismann, V., Herver, A. and König-Langlo, G.: One year of particle size distribution
27 and aerosol chemical composition measurements at the Zeppelin station, Svalbard,
28 March 2000-2001, *Phys. Chem. Earth*, 28, 1181-1190, 2003.

29 Sun, L., Li, X., Hede, T., Tu, Y., Leck, C., and Ågren, H.: Molecular dynamics
30 simulations reveal the assembly mechanisms of polysaccharides in marine aerosols,
31 *Phys. Chem. Chem. Phys.*, 16, 25935-25941, 2014.

1 Tanaka, T., Fillmore, D., Sun, S., Nishio, I., Wislow, G. S., Shah, A.: Phase
2 transitions in ionic gels, *Phys. Rev. Lett.* 45, 1636-1642, 1980.

3 Tjernström, M., Leck, C., Birch, C. E., Bottenheim, W. E., Brooks, B. J., Brooks, I.
4 M., Bäcklin, L., Chang, R. Y.-W., Granath, E., Graus, M., Hansel, A., Heintzenberg,
5 J., Held, A., Hind, A., de la Rosa, S., Johnston, P., Knulst, J., de Leuuw, G., di
6 Liberto, L., Martin, M., Matrai, P. A., Mauritsen, T., Müller, M., Norris, S. J.,
7 Orellana, M. V., Orsini, D. A., Paatero, J., Persson, P. O. G., Gao, Q., Rauschenberg,
8 C., Ristovski, Z., Sedlar, J., Shupe, M. D., Sireau, B., Sirevaag, A., Sjogren, S.,
9 Stetzer, O., Swietlicki, E., Szczodrak, M., Vaattovaara, P., Wahlberg, N., Westberg,
10 M., and Wheeler, C. R.: The Arctic Summer Cloud-Ocean Study (ASCOS): overview
11 and experimental design, *Atmos. Chem. Phys.*, 14, 2823–2869, doi:10.5194/acp-14-
12 2823-2014, 2014.

13 Twomey, S. A.: The influence of pollution on the shortwave albedo of clouds, *J.
14 Atmos. Sci.*, 34, 1149-1152, 1977.

15 Verdugo, P.: Marine microgels, *Annu. Rev. Mar. Sci.*, 4, 375-400, 2012.

16 Verdugo, P., Alldredge, A. L., Azam, F., Kirchman, D. L., Passow, U., and Santschi,
17 P. H.: The oceanic gel phase: a bridge in the DOM-POM continuum, *Mar. Chem.* 92,
18 67-85, 2004.

19 Wiedensohler, A., Birmili, W., Nowak, A., Sonntag, A., Weinhold, K., Merkel, M.,
20 Wehner, B., Tuch, T., Pfeifer, S., Fiebig, M., Fjäraa, A. M., Asmi, E., Sellegrí, K.,
21 Depuy, R., Venzac, H., Villani, P., Laj, P., Aalto, P., Ogren, J. A., Swietlicki, E.,
22 Williams, P., Roldin, P., Quincey, P., Hüglin, C., Fierz-Schmidhauser, R., Gysel, M.,
23 Weingartner, E., Riccobono, F., Santos, S., Grüning, C., Faloon, K., Beddows, D.,
24 Harrison, R., Monahan, C., Jennings, S. G., O'Dowd, C. D., Marinoni, A., Horn, H.-
25 G., Keck, L., Jiang, J., Scheckman, J., McMurry, P. H., Deng, Z., Zhao, C. S.,
26 Moerman, M., Henzing, B., de Leeuw, G., Löschau, G., and Bastian, S.: Mobility
27 particle size spectrometers: harmonization of technical standards and data structure to
28 facilitate high quality long-term observations of atmospheric particle number size
29 distributions, *Atmos. Meas. Tech.*, 5, 657–685, doi:10.5194/amt-5-657-2012, 2012.

30 Williams, D. B. and Carter, C. B.: *Transmission Electron Microscopy, A textbook for
31 materials science, Part I: Transmission electron microscopy*, Springer Science +
32 Buisness Media, New York, USA, p. 354 ff., 1996.

1 Winiger, P., Andersson, A., Yttri, K. E., Tunved, P., and Gustafsson, Ö.: Isotope-based source appointment of EC aerosol particles during winter high-pollution events
2 at the Zeppelin Observatory, Svalbard, Environ. Sci. Techol., 49, 11959-11966, doi:
3 10.1021/acs.est.5b02644, 2015.

5 Xie, Z., Blum, J. D., Utsunomiya, S., Ewing, R. C., Wang, X., and Sun, L.:
6 Summertime carbonaceous aerosols collected in the marine boundary layer of the
7 Arctic Ocean, Journal of Geophysical Research, 112(D2), 2007.

8 Xin, L., Leck, C., Sun, L., Hede, T., Tu, Y. and Ågren, H.: Cross-linked
9 polysaccharide assemblies in marine gels: an atomistic simulation, J. Phys. Chem.
10 Lett., 4, 2637-2642, doi: 10.1021/jz401276r, 2013.

11 Zhou, J., Swietlicki, E., Berg, O. H., Aalto, P. P., Hämeri, K., Nilsson, E. D. and
12 Leck, C.: Hygroscopic properties of aerosol particles over the central Arctic Ocean
13 during summer, J. Geophys. Res., 106, 32111-32123, 2001.

14 Zhou, J., Mopper, K. and Passow, U.: The role of surface-active carbohydrates in the
15 formation of transparent exopolymer particles by bubble adsorption of seawater,
16 Limnol. Oceanogr., 43, 1860-1871, 1998.

17 Zhou, W., Apkarian, R., Wang, Z. L., and Joy, D.: Fundamentals of scanning electron
18 microscopy, in: Scanning Microscopy for Nanotechnology - Techniques and
19 Applications [Zhou, W. and Wang, Z. L. (eds.)], Springer Business + Media, New
20 York, 2006.

21

22

1

	15-80 nm	80-200 nm	> 200 nm	Sum (% of total)
Single particles (% of total SP)	2609 (80%)	573 (18%)	57 (2%)	3239 (82 %)
Gel particles (% of total GP)	97 (24%)	198 (49%)	108 (27%)	403 (11 %)
Halo particles (% of total HP)	9 (3%)	95 (36%)	163 (61%)	267 (7 %)
Total number of particles			3909 (100%)	

2 Table 1. Numbers and percentage of total for single particles (SP), gel particles (GP)
3 and halo particles (HP) imaged with SEM and used for calculating the number size
4 distributions.

5

	No Na^+/K^+ no $\text{Ca}^{2+}/\text{Mg}^{2+}$	$\text{Ca}^{2+}/\text{Mg}^{2+}$	Na^+/K^+	$\text{Ca}^{2+}/\text{Mg}^{2+}$ and Na^+/K^+
Single particles	4 %	4 %	13 %	78 % (Na^+/K^+)
“Aggregate” particles	-	-	20 %	80 % (Na^+/K^+)
“Aggregate with film” particles	-	17 %	17 %	67% ($\text{Ca}^{2+}/\text{Mg}^{2+}$)
“Mucus-like” particles	-	11 %	3 %	86 % ($\text{Ca}^{2+}/\text{Mg}^{2+}$)
Halo particles	25 %	-	50 %	25 % (Na^+/K^+)

Table 2. Fraction of particles containing the ions Na^+/K^+ or $\text{Ca}^{2+}/\text{Mg}^{2+}$, or both Na^+/K^+ and $\text{Ca}^{2+}/\text{Mg}^{2+}$, or neither Na^+/K^+ nor $\text{Ca}^{2+}/\text{Mg}^{2+}$ in single particles, “aggregate” particles, “aggregate with film” particles, “mucus-like” particles and halo particles. The ions written in brackets in the last column indicate the prevalent type of ion in the respective type of particle.

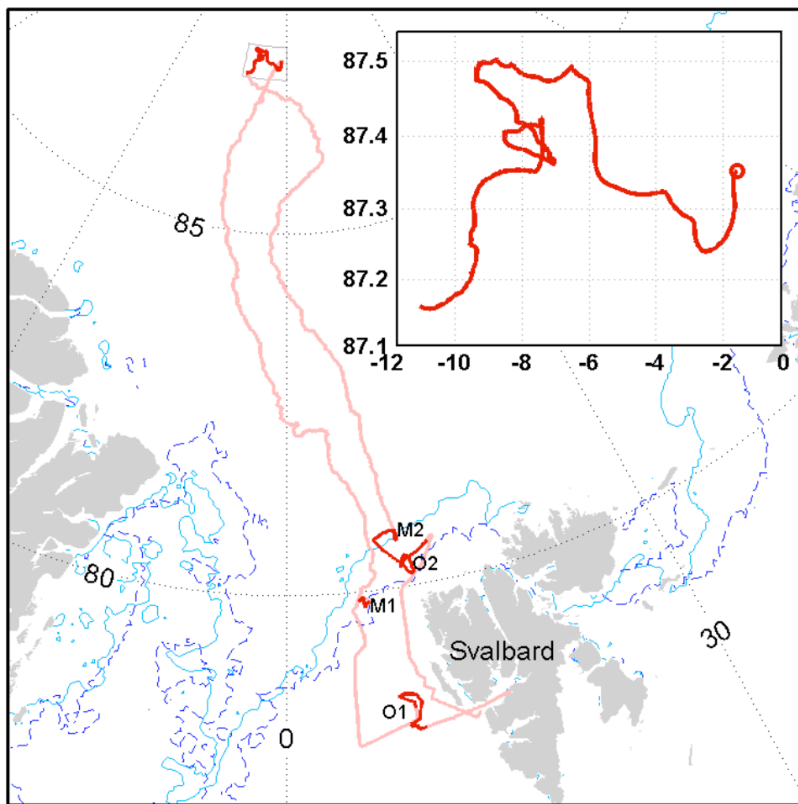


Figure 1. Track of the icebreaker *Oden* in the Arctic (pink). The path during the ice-drift is shown in the insert (red line); the circle indicates the start of the ice-drift, the ice edge (thin blue line) was passed on 12 August 2008.

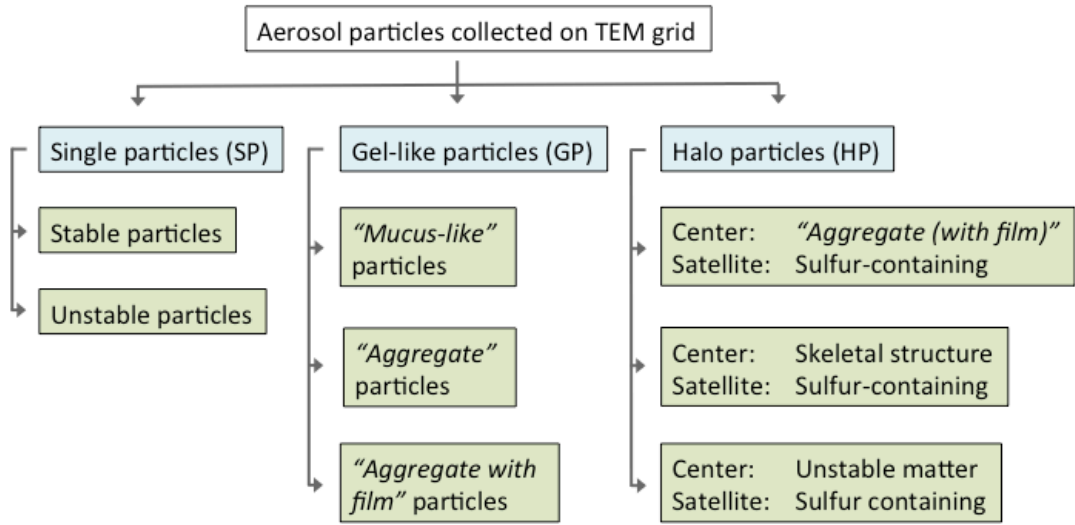


Figure 2. Scheme of the aerosol particle types collected on Formvar grid; the particles observed with SEM are shaded in light blue, and particles observed in TEM are shaded in light green.

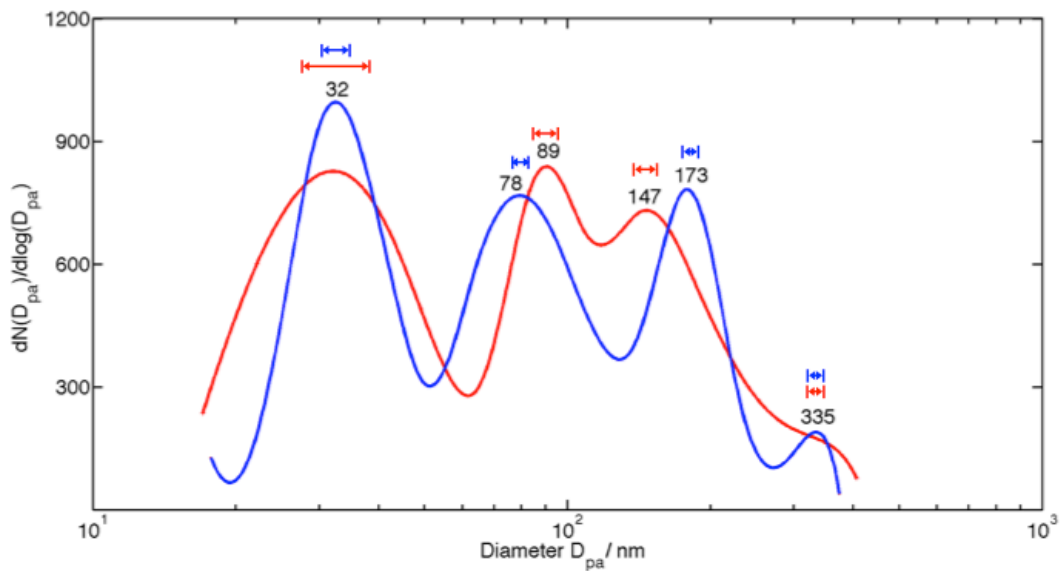


Figure 3. Number size distribution of the total aerosol collected for this study with the red line representing the SEM derived particle number distribution, and the red error bars representing the error in size determination retrieved from calibration measurements described in Hamacher-Barth et al. (2013). The blue line depicts the number size distribution from simultaneous Tandem Differential Mobility Particle Sizer measurements, and the blue error bars depict a 5% uncertainty of the data (Wiedensohler et al., 2012).

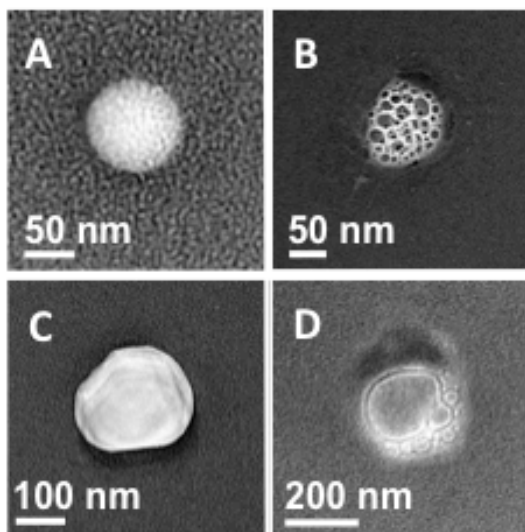


Figure 4. Examples for single particles (SP) observed with TEM: (A) A particle stable under the beam of the electron microscope; (B) a particle with a skeletal structure; (C) a particle stable under the electron beam; and (D) an example for a particle that is unstable under the electron beam.

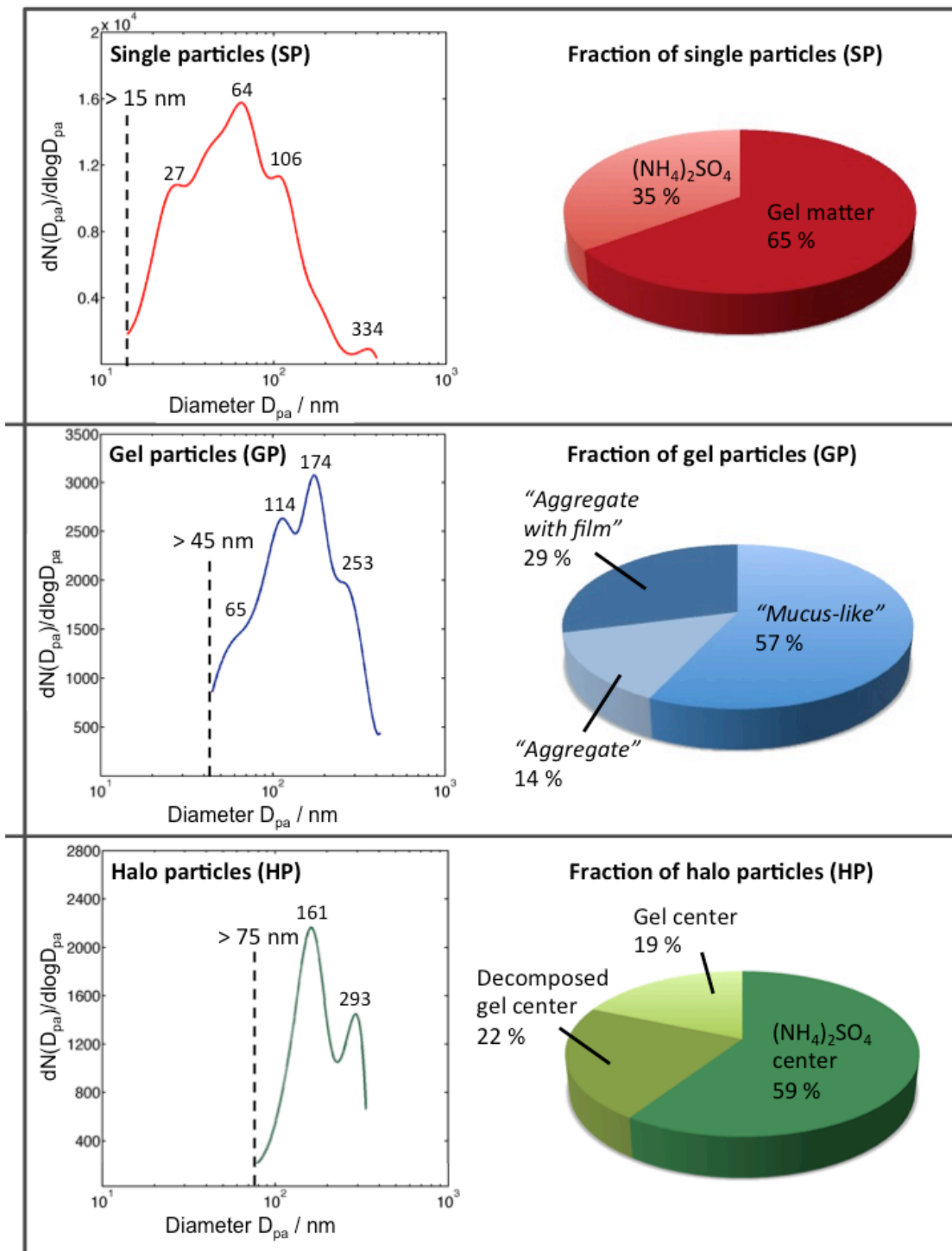


Figure 5. SEM number size distribution of the particle types (single particles, gel-like particles and halo particles) evaluated for this study (on the left) plus the fraction of the different subgroups of particles derived from TEM (on the right). The dashed line in each figure marks the lowest diameter at which the respective particle type appears.

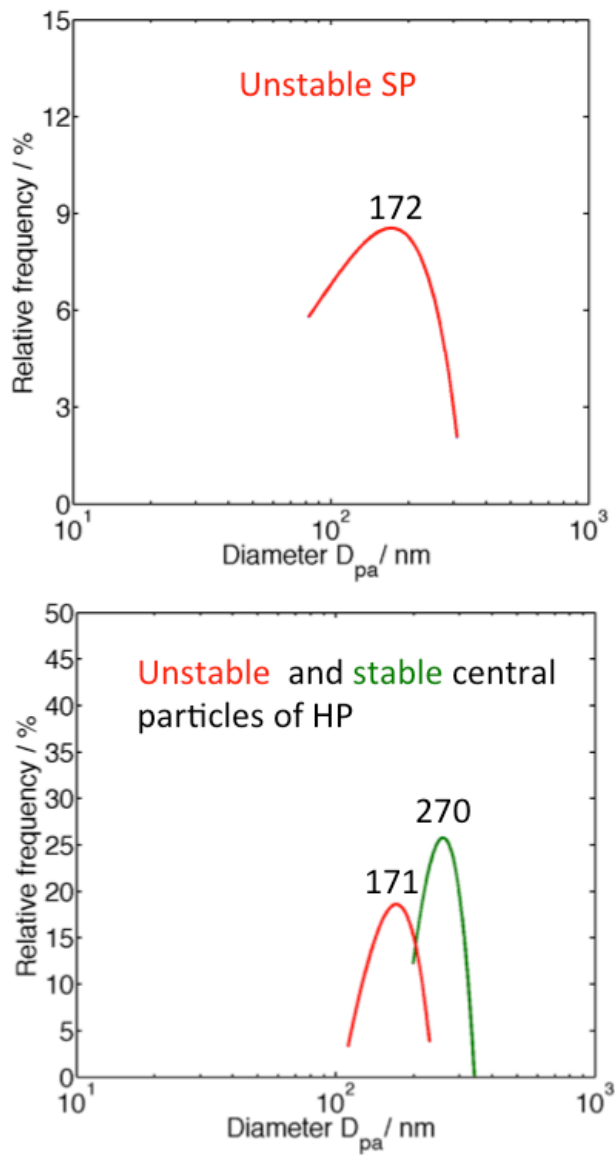


Figure 6. Number size distributions obtained from TEM images. Upper panel shows unstable SP while the lower panel exhibits central particles of HP. The red line represents the unstable central particles, while the green line represents the stable central particles comprising “aggregate”, “aggregate with film” and skeletal particles.

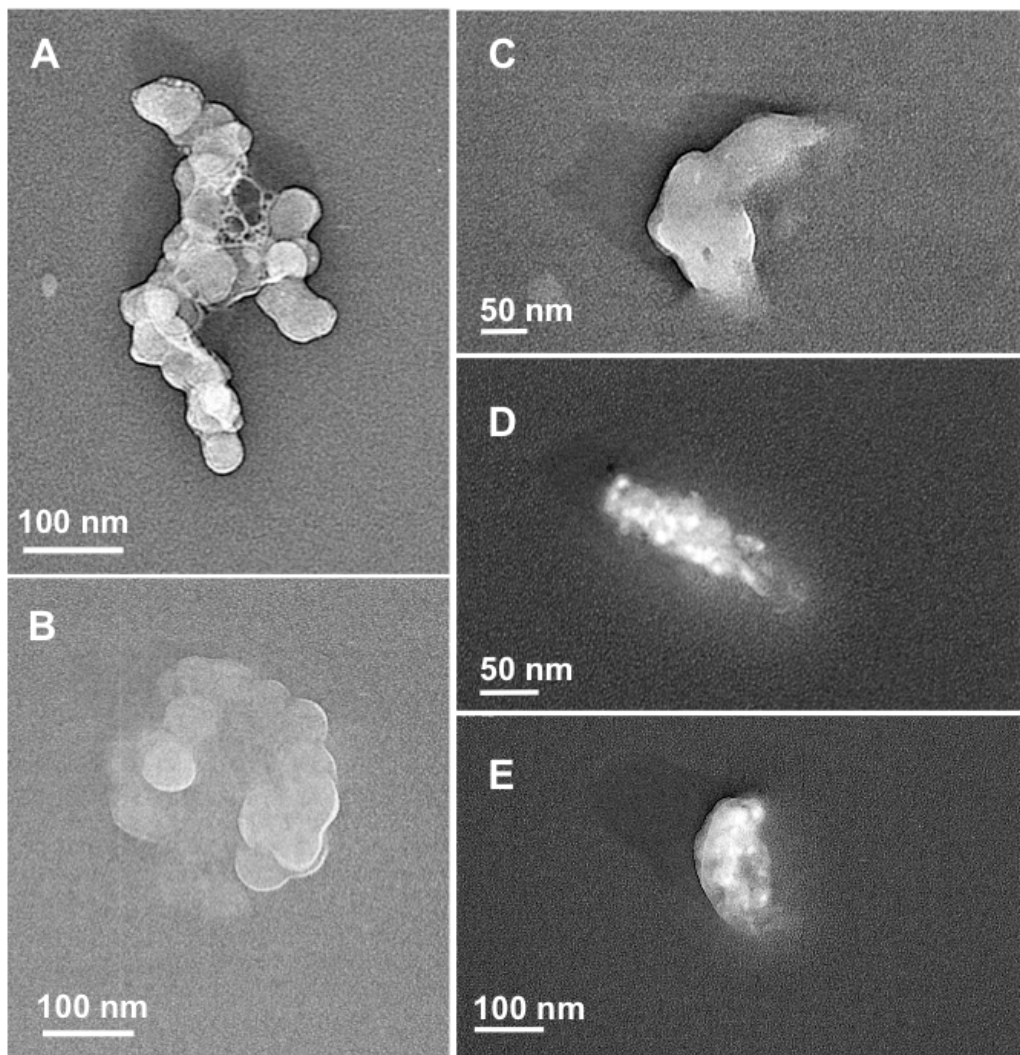


Figure 7. Examples for particles built up by aggregated subunits, observed with TEM: (A), (B) pure *“aggregate”* particles; (C), (D) and (E) aggregate particles covered with a thin film of gel *“aggregate with film”* particles.

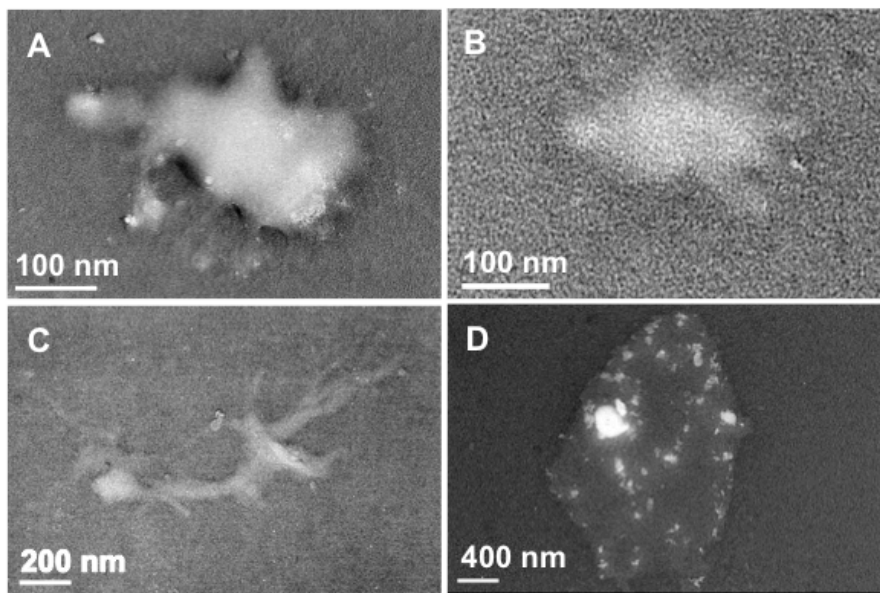


Figure 8. Examples for “*mucus-like*” particles observed with TEM: (A) mucus matter with small dense inclusions, partly outdrawn on the Formvar film; (B) mucus matter without dense inclusions; (C) mucus matter, extensively outdrawn on the formvar film; (D) mucus matter with numerous small dense inclusions.

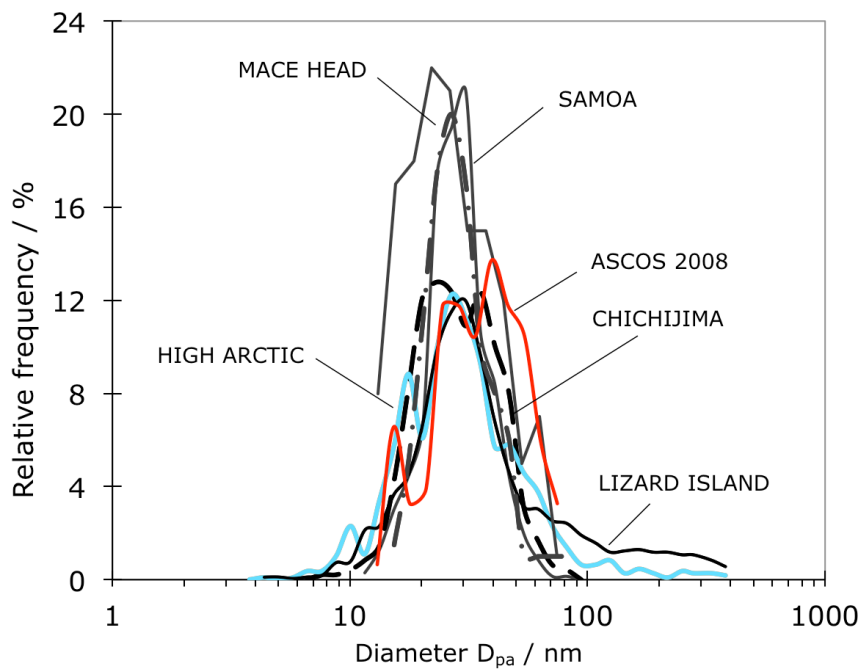


Figure 9. Number size distributions of airborne aggregate particles and their building blocks at different locations: Mace Head (53°N , 10°W), Lizard Island (14.6°S , 145.5°E), American Samoa (14°S , 172°W), Chichijima (27°N , 142°E), High Arctic (AOE-2001, between 88.9°N and 88.2°N ; light blue line), and ASCOS 2008 (between 87°N , 1°W and 87°N , 11°W , red line). All particles were assumed to be spherical in shape (from Bigg and Leck (2008), modified).

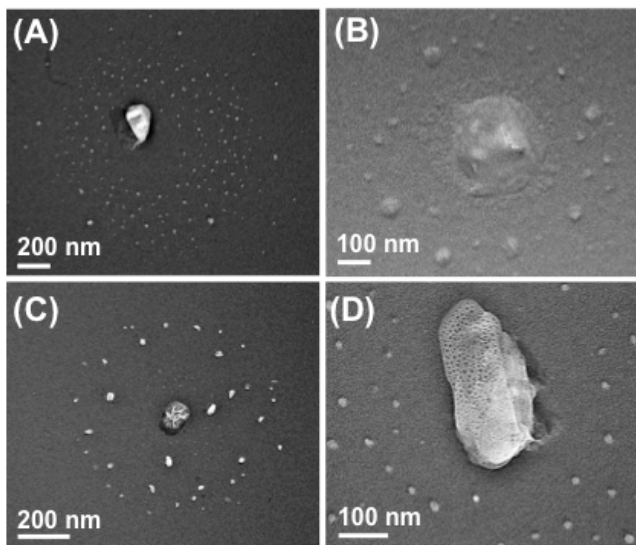


Figure 10. Examples for Halo Particles observed with TEM. (A) a central “aggregate” particle surrounded by satellite particles of sulfuric acid and a smaller amount of methane sulfonic acid. (B) a central particle of “aggregate with film”, surrounded by satellite particles of sulfuric acid and methane sulfonic acid. (C) a central particle of ammonium sulfate, satellite particles formed by methane sulfonic acid, probably mixed with sulfuric acid. (D) a central particle of degenerated gel, surrounded by methane sulfonic acid mixed with sulfuric acid.

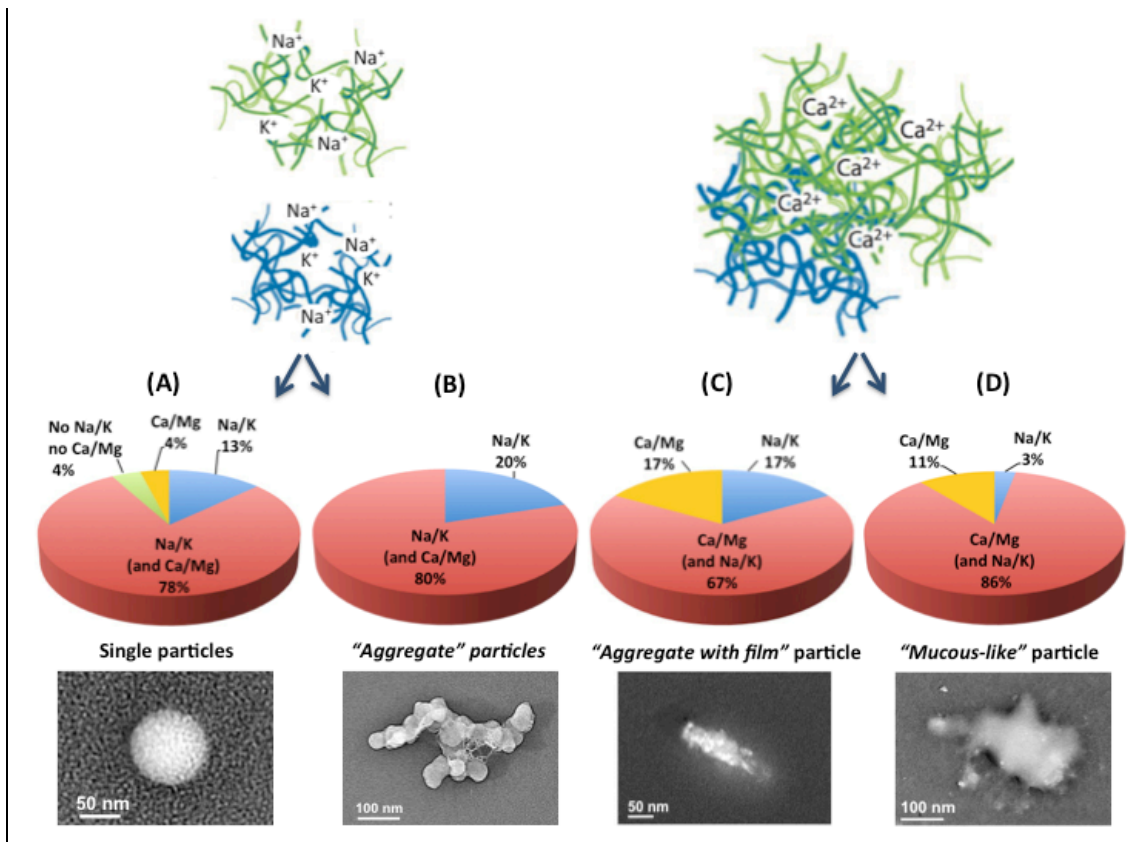


Figure 11. Fraction of particles containing the following ions: Na^+/K^+ (blue), $\text{Ca}^{2+}/\text{Mg}^{2+}$ (yellow), Na^+/K^+ and minor contents of $\text{Ca}^{2+}/\text{Mg}^{2+}$ (red), and neither Na^+/K^+ nor $\text{Ca}^{2+}/\text{Mg}^{2+}$ (green). (A) Single particles comprised of gel matter. (B) “*mucus-like*” particles. (C) “*aggregate*” particles. (D) “*aggregate with film*” particles.

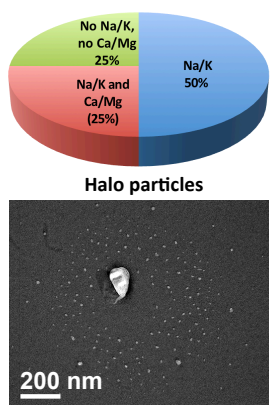


Figure 12. Fraction of HP containing the following ions: Na^+/K^+ (blue), Na^+/K^+ and $\text{Ca}^{2+}/\text{Mg}^{2+}$ (red), and neither Na^+/K^+ nor $\text{Ca}^{2+}/\text{Mg}^{2+}$ (green).

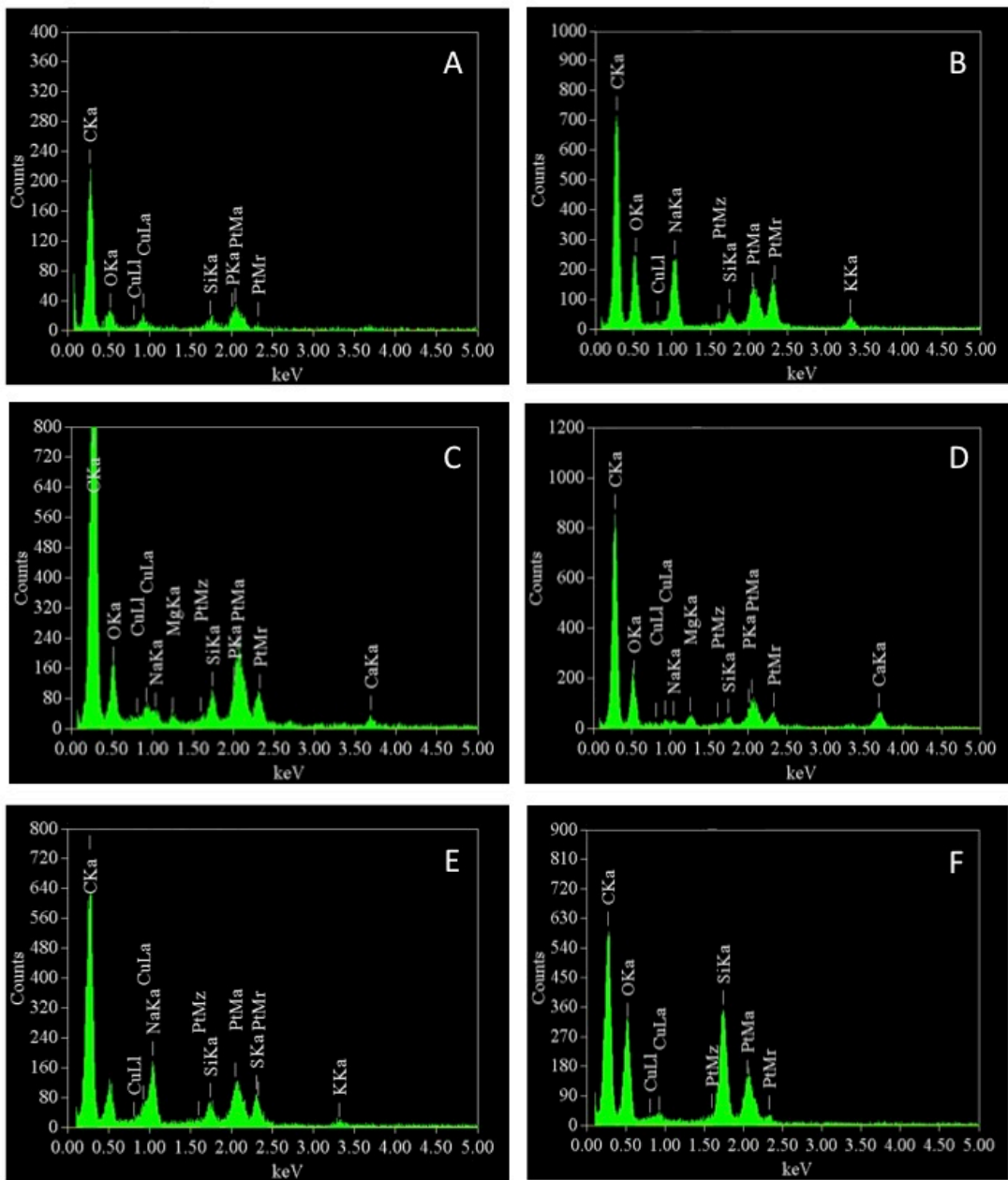


Figure S1: Examples of EDX spectra of aerosol particle investigated in this study: (A) single particle containing neither Na^+/K^+ nor $\text{Ca}^{2+}/\text{Mg}^{2+}$; (B) “aggregate” particle containing Na^+/K^+ ; (C) “aggregate with film” particle containing Na^+ and minor contents of $\text{Ca}^{2+}/\text{Mg}^{2+}$; (D) “mucus-like” particle containing $\text{Ca}^{2+}/\text{Mg}^{2+}$ and minor contents of Na^+ ; (E) halo particle containing Na^+/K^+ and S probably in the satellite particles; (F) blank spectrum taken from a Pt-shadowed TEM grid.

